

Final Ti Model Results

Tigany Zarrouk

April 6, 2020

Contents

1	Objective Function	2
2	Phonons	4
2.1	Harmonic	4
2.2	Quasiharmonic Effects	4
2.2.1	Gibbs free energy	4
2.2.2	Thermal Expansion	5
3	Defect Clusters	6
3.1	Octahedral O interstitial relaxation	6
3.2	Tetrahedral O interstitial relaxation	7
3.3	Energies for defects	9
3.4	All formation energies	10
4	Binding energy of defect clusters in the harmonic approximation	11
5	Gamma surfaces	11
5.1	Basal	12
5.2	Prismatic	12
5.3	Pyramidal first order	14
5.4	Data	16
6	Dislocation core structures	17
6.1	Quadrupolar Array	17
6.1.1	Methodology	17
6.1.2	Discussion	17
6.1.3	TODO Dissociation Distance Analysis	18
6.1.4	TODO Disregistry Analysis	19
6.1.5	IP1	21
6.1.6	IP2	22
6.1.7	IP3	23
6.1.8	IP4	24
6.1.9	IP5	25
6.1.10	Ghazisaeidi Results for comparison	26
6.1.11	TODO Replot all dislocations and do analysis in Atomman.	26
6.1.12	Peierls Stress	26
6.1.13	Data	29
6.1.14	Directory of the results	29
6.2	Cluster Method	29

6.2.1	Methodology	29
6.2.2	Circular Cluster	30
6.2.3	Hexagonal Cluster	30
6.2.4	Peierls Stress	30
6.2.5	Discussion	32
7	Binding of oxygen to dislocations	32
7.1	Quadrupolar Array	32
7.2	Notes	34
7.3	Dissolution Energy Equation	34
7.4	Current status of simulation	35
8	Peierls Barriers	35
9	BOP	35
9.1	4 recursion levels	35
10	Bibliography	36

1 Objective Function

```

PARAMETERS fdd=0.1958363809 qdds=0.5591275855 qddp=0.5690351902 qddd=0.7745947522 b0=58.0906936439
p0=1.2185323579 b1=-3.2299188646 p1=0.6862915307 b2=593519.1134129359 m2=-11.5000000000 p2=0.0000000000
ndt=2.0000000000 cr1=-6.0000000000 cr2=3.0474400934 cr3=-1.2317472193 r1dd=6.5000000000 rcdd=10.0000000000
rmaxhm=10.1000000000 npar=18 VARGS -vfdd=0.1958363809 -vqdds=0.5591275855 -vqddp=0.5690351902
-vqddd=0.7745947522 -vb0=58.0906936439 -vp0=1.2185323579 -vb1=-3.2299188646 -vp1=0.6862915307 -
vb2=593519.1134129359 -vm2=-11.5000000000 -vp2=0.0000000000 -vnndt=2.0000000000 -vcr1=-6.0000000000
-vcr2=3.0474400934 -vcr3=-1.2317472193 -vr1dd=6.5000000000 -vrccdd=10.0000000000 -vrmaxhm=10.1000000000

```

Quantity	From Model	Target
a _{hcp}	5.58523112	5.57678969
c/a	1.58371266	1.58731122
a _{omega}	8.93475285	8.73254342
c _{omega}	5.38726911	5.32343103
a _{4h}	5.57584691	5.56325146
c _{4h}	18.09810672	17.75908031
a _{6h}	5.57365569	5.54639384
c _{6h}	27.18378460	26.77136353
a _{bcc}	6.20079768	6.17948863
a _{fcc}	7.87290654	7.88677000
DE(o,h)	0.58764167	-0.63343333
DE(4h,h)	1.58019500	3.17160000
DE(6h,h)	2.48264833	3.72005000
DE(b,h)	5.35128500	7.63520000
DE(f,h)	3.78088500	4.51880000
c ₁₁	171.60928873	176.10000000
c ₃₃	198.90063708	190.50000000
c ₄₄	47.42549704	50.80000000
c ₁₂	94.65941969	86.90000000
c ₁₃	61.22624060	68.30000000
M _{freq0}	2.59341377	2.85858719
M _{freq1}	2.59341378	2.85858719
M _{freq2}	2.59341378	2.85858719
M _{freq3}	2.59341379	2.85858719
M _{freq4}	5.85272461	5.66706047
M _{freq5}	5.85272461	5.66706047
H _{freq0}	3.82320403	4.80643423
H _{freq1}	3.82320403	5.58010025
H _{freq2}	6.40288977	5.65316738
H _{freq3}	6.40288977	6.36651842
H _{freq4}	7.92857431	6.40050186
H _{freq5}	7.92857431	7.64082373
bandw. G	3.69394702	5.87085872
bandw. K	4.65178817	4.97424321
bandw. M	5.19329495	7.78109872
bandw. L	4.21232412	6.34433701
bandw. H	3.54700549	9.70902614
DOSerr _h	0.00000000	0.00000000
DOSerr _o	0.00000000	0.00000000
E _{prisf}	98.95340236	220.00000000

— E_{prismaticfault} —

tbe:	98.953	mJ/m ²
DFT:	250.000	mJ/m ² [Benoit 2012]
DFT:	233.000	mJ/m ² [Ackland 1999]

— E_{Basalfault I2} —

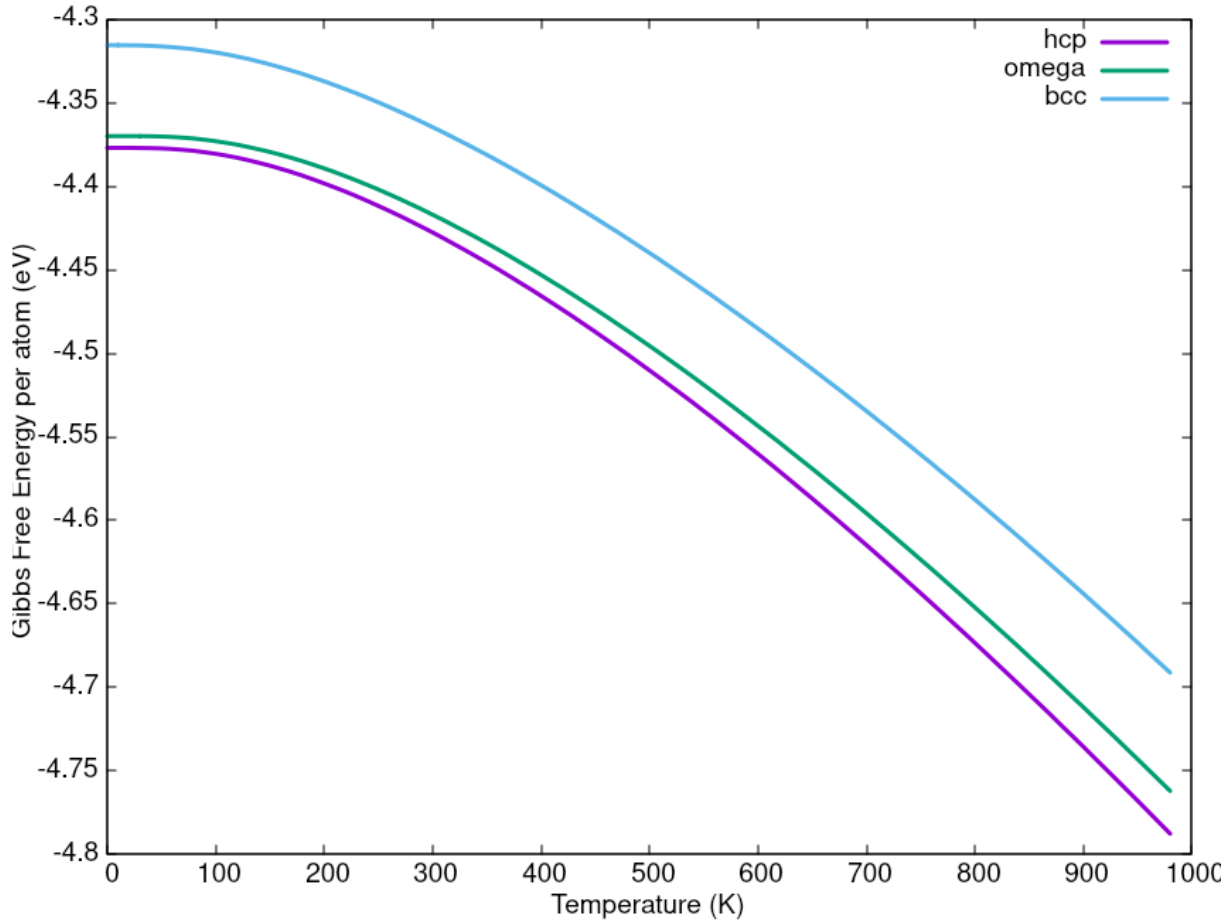
tbe:	211.658	mJ/m ²
DFT:	260.000	mJ/m ² [Benoit 2012]

2 Phonons

2.1 Harmonic

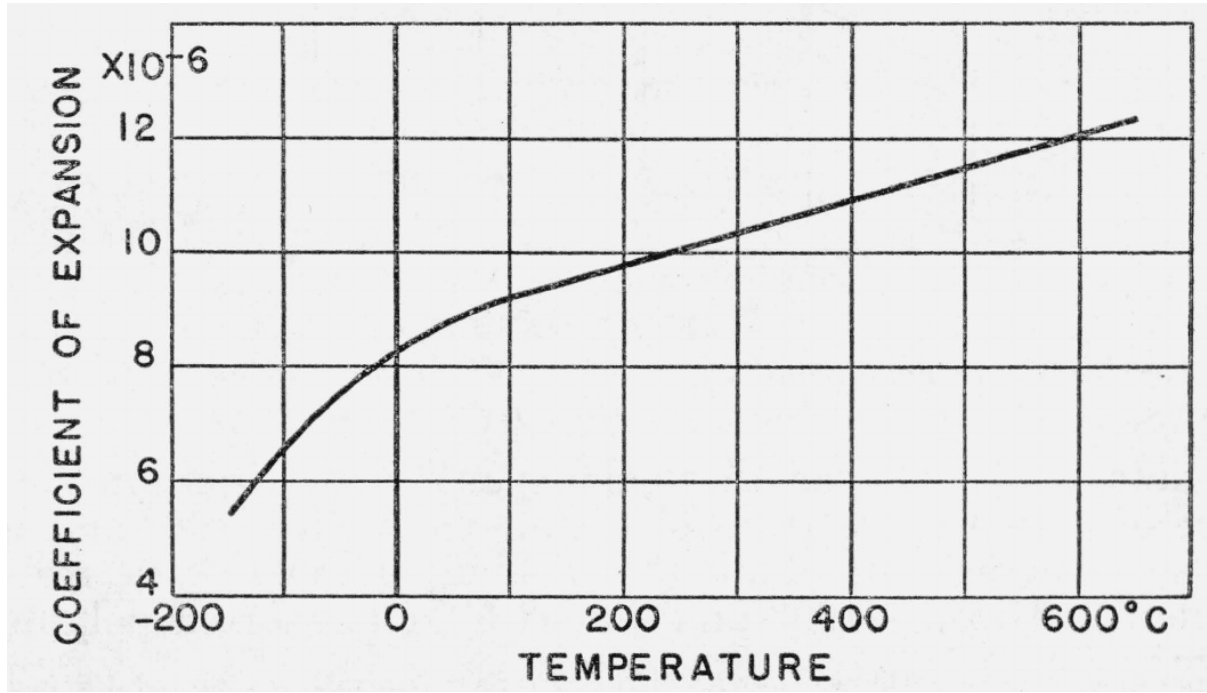
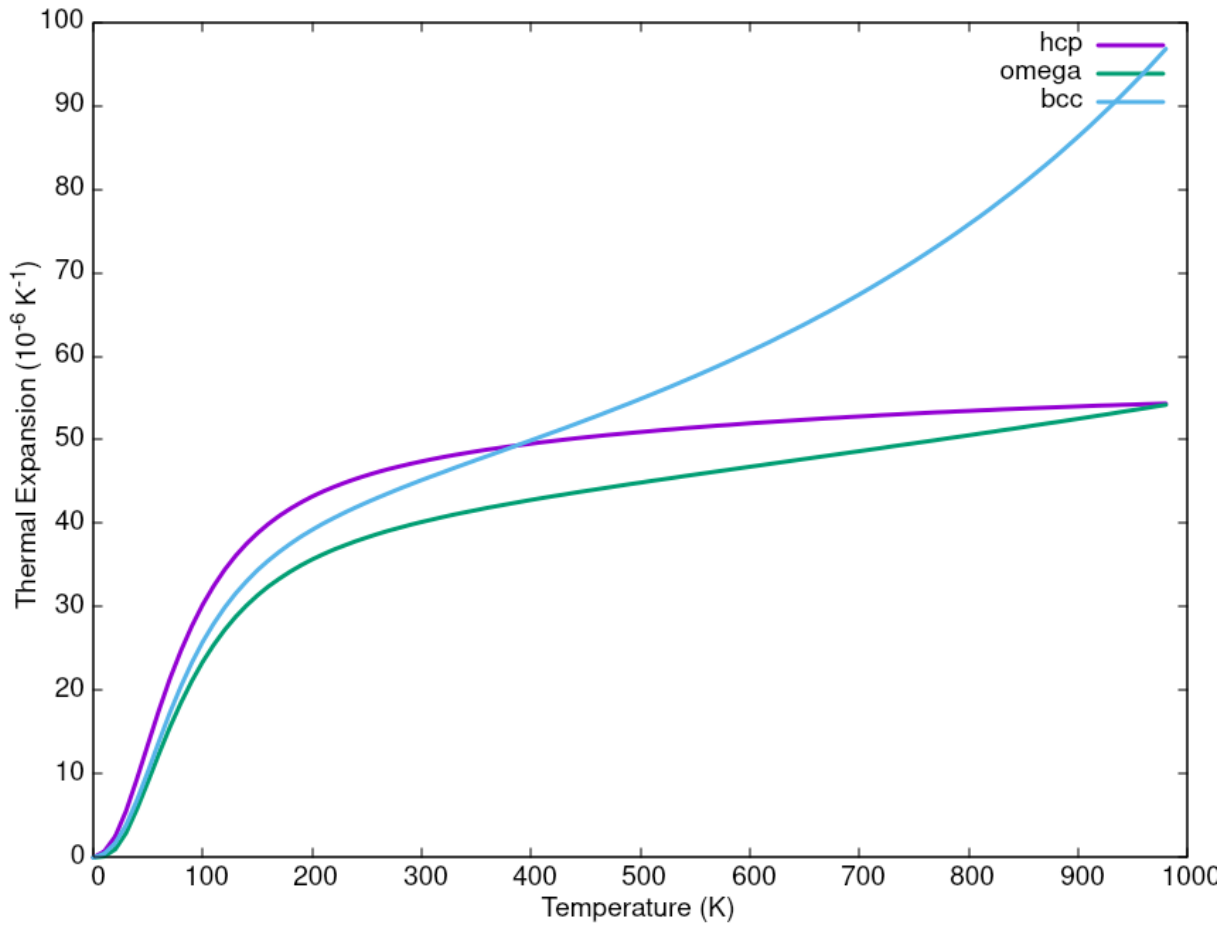
2.2 Quasiharmonic Effects

2.2.1 Gibbs free energy



- This does NOT take into account configurational entropy, but this

2.2.2 Thermal Expansion



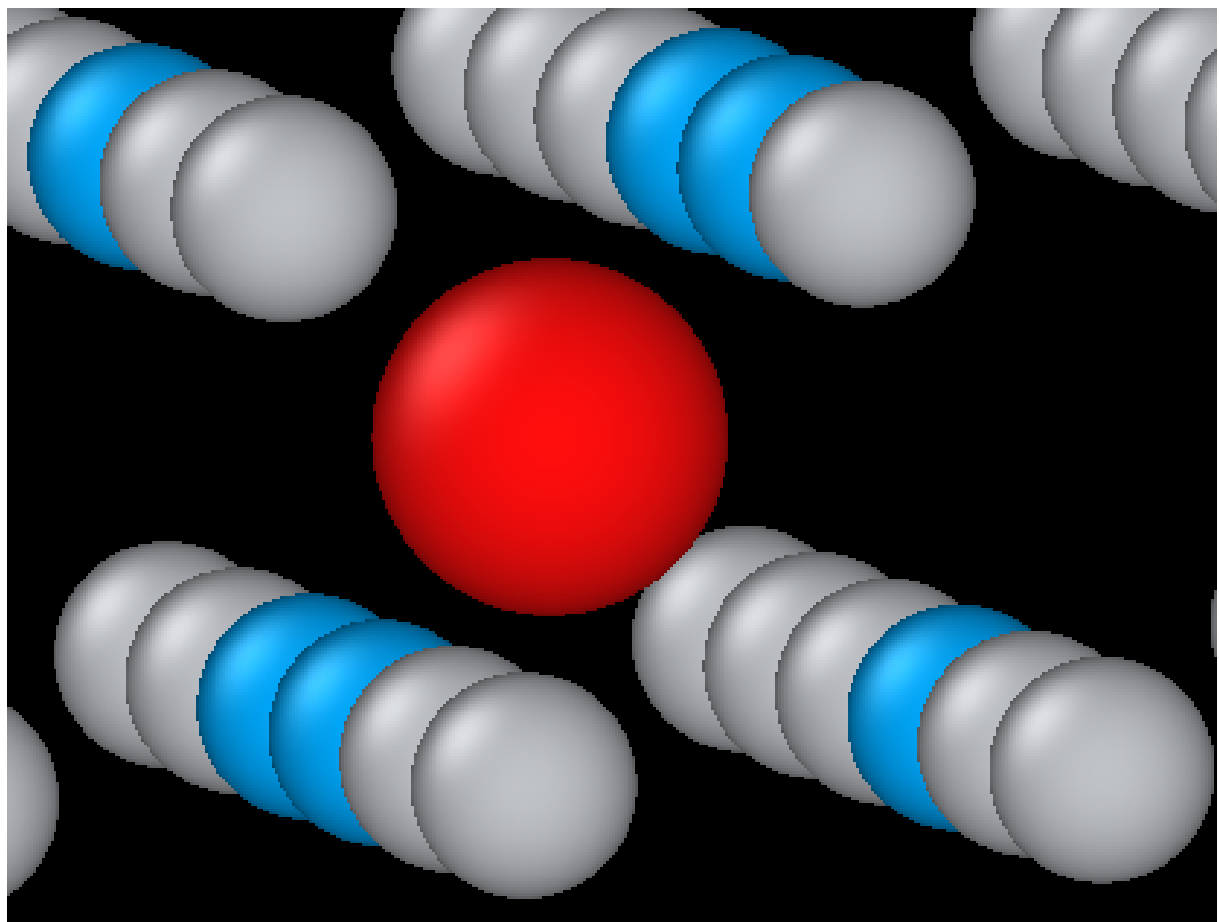
3 Defect Clusters

— $E_{\text{vacancyformation}}$ —

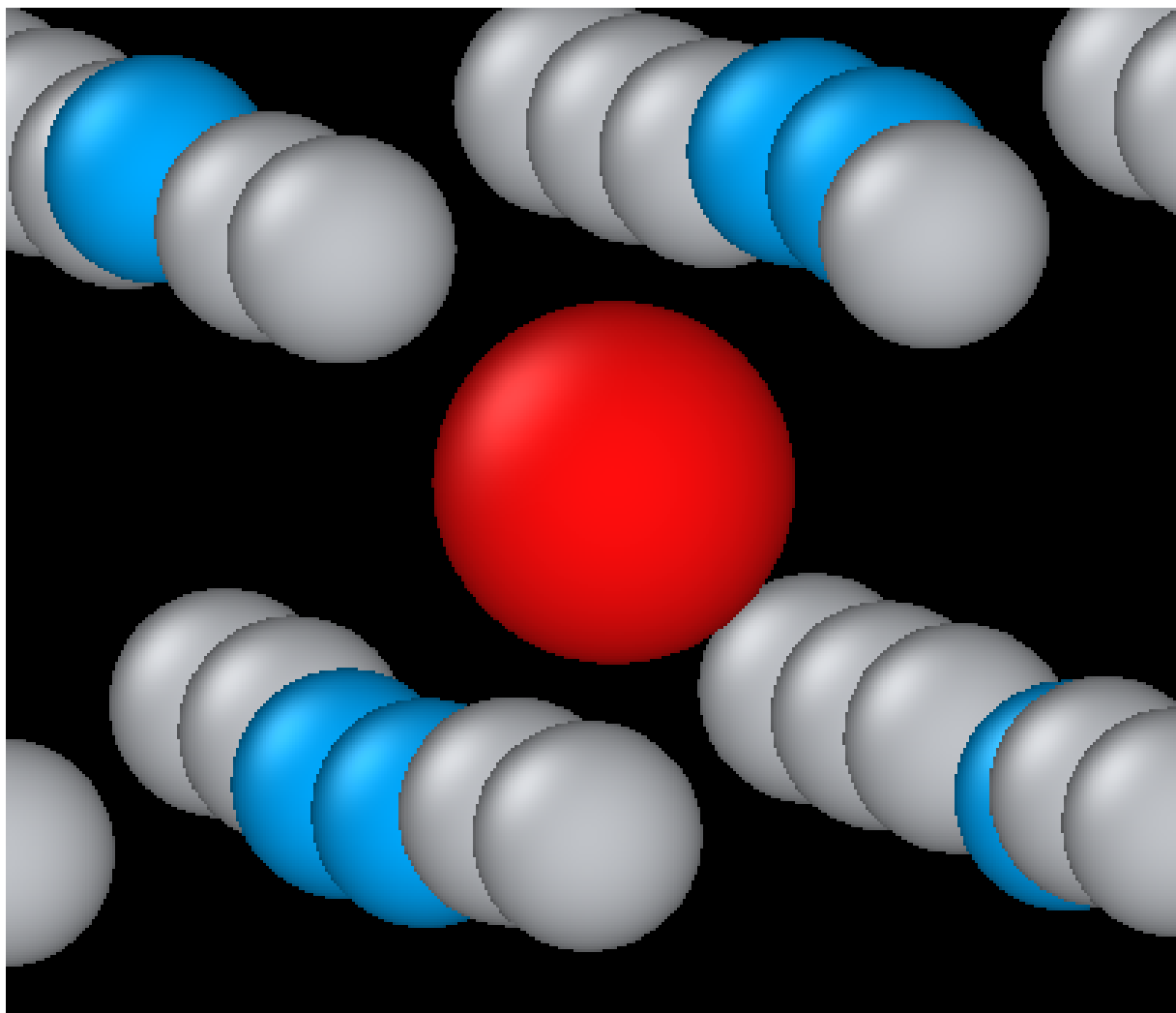
tbe: 2.347 eV
DFT: 1.950 eV GGA-PAW: Angsten (2013)
exp: 1.270 eV Hashimoto (1984)

3.1 Octahedral O interstitial relaxation

Initial:

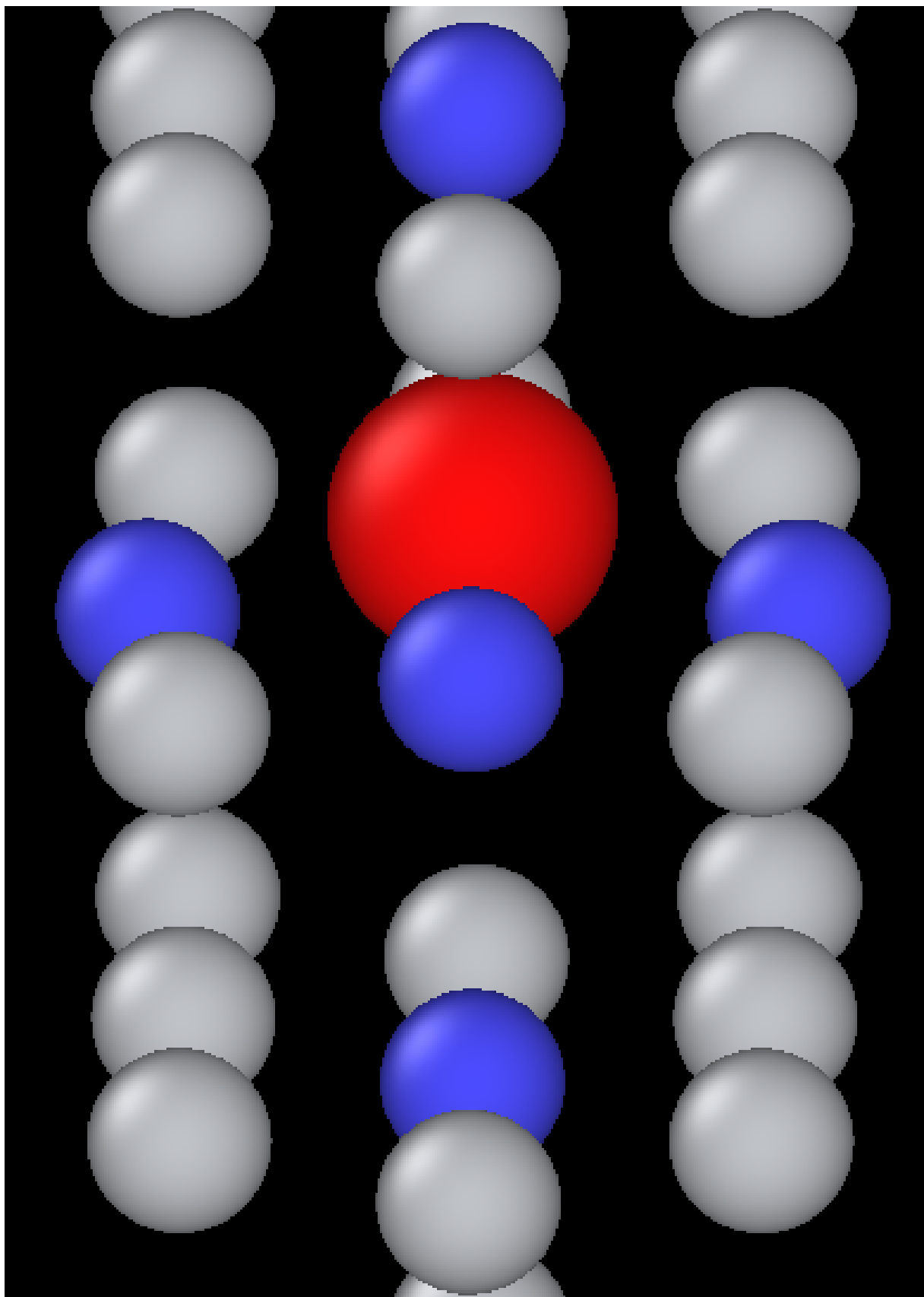


Final:

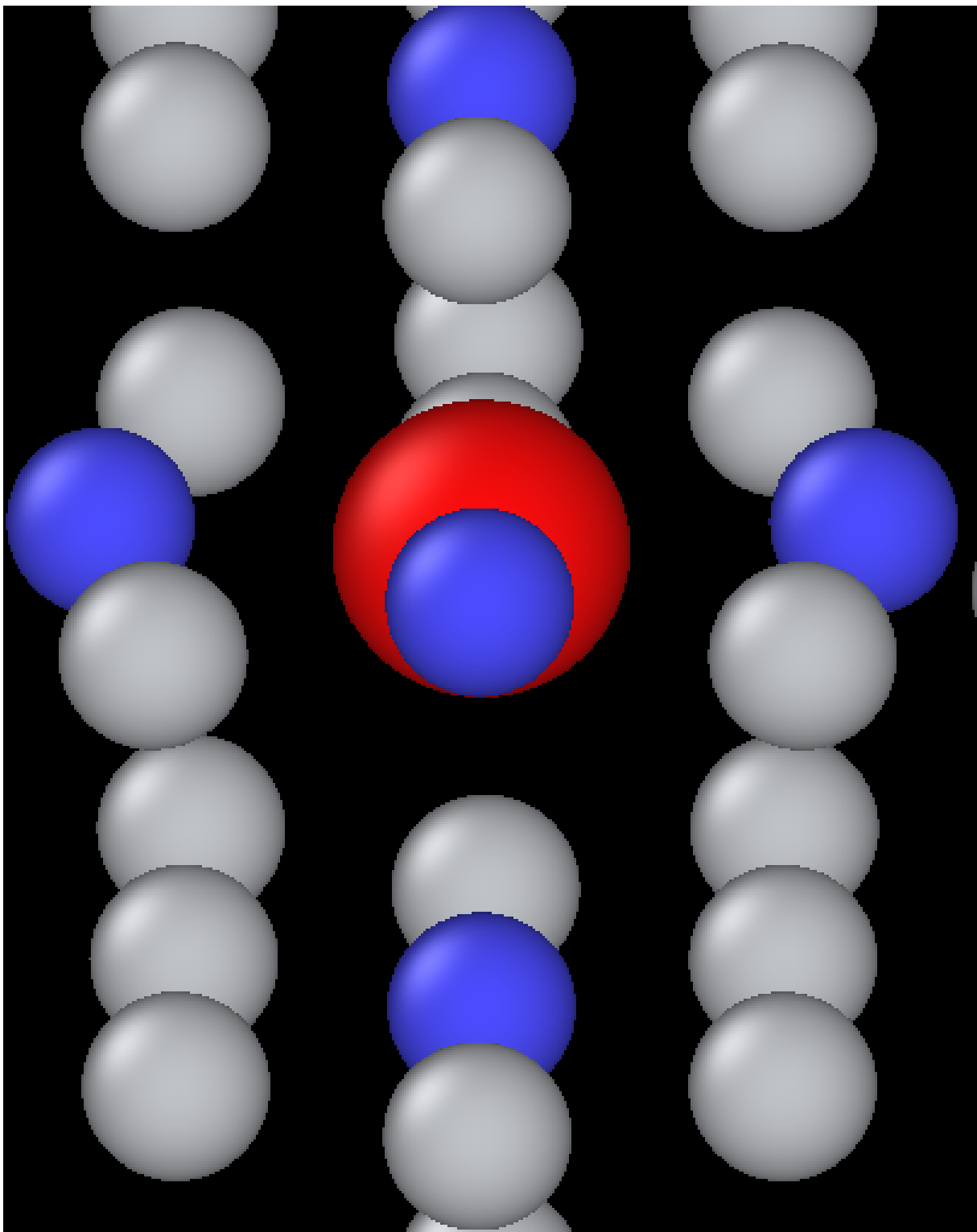


3.2 Tetrahedral O interstitial relaxation

Initial:



Final:



3.3 Energies for defects

Relative differences are

$$\gg (E_{\text{tetrahedral}} - E_{\text{octahedral}})$$

tbe: 1.65 eV

GGA-DFT: 1.23 eV Kwasniak (2013)

$$\gg (E_{\text{hexahedral}} - E_{\text{octahedral}})$$

tbe: 0.90 eV

> Note: Preference for tetrahedral oxygen to go into hexahedral site as seen by images above
 All formation energies below use the chemical potential of Akysonov (2013) of value $\mu_{\text{oxygen}} = \frac{5.6}{2} eV$.

3.4 All formation energies

Quantity	Energy (eV)
Ef _{Vf}	2.347
Ef _{Tsol}	- 21.783
Ef _{Osol}	- 23.436
Ef _{OOsol}	- 49.606
Ef _{OOOsol}	- 76.037
Ef _{OOOOsol}	- 102.470
Ef _{OOOOOsol}	- 128.781
Ef _{OOOOOOsol}	- 155.148
Ef _{Tdilimp}	- 28.991
Ef _{Odilimp}	- 30.645
Ef _{OODilimp}	- 56.814
Ef _{OOOdilimp}	- 83.246
Ef _{OOOOdilimp}	- 109.679
Ef _{OOOOOdilimp}	- 135.989
Ef _{OOOOOOdilimp}	- 162.357
Ef _{Tformation}	- 21.783
Ef _{Oformation}	- 23.436
Ef _{OOformation}	- 46.806
Ef _{OOOformation}	- 70.437
Ef _{OOOOformation}	- 94.070
Ef _{OOOOOfomation}	- 117.581
Ef _{OOOOOOformation}	- 141.148
Ef _{TVformation}	- 18.905
Ef _{OVformation}	- 18.905
Ef _{OOVformation}	- 41.910
Ef _{OOOVformation}	- 66.013
Ef _{OOOOVformation}	- 88.998
Ef _{OOOOOVformation}	- 113.649
Ef _{OOOOOOVformation}	- 137.110
Ef _{Tvacsolbind}	- 0.530
Ef _{Ovacsolbind}	- 2.183
Ef _{OOvacsolbind}	- 2.547
Ef _{OOOvacsolbind}	- 2.076
Ef _{OOOOvacsolbind}	- 2.724
Ef _{OOOOOvacsolbind}	- 1.583
Ef _{OOOOOOvacsolbind}	- 1.690

4 Binding energy of defect clusters in the harmonic approximation

Using the defect cluster configurations mentioned earlier, one can find the change in defect cluster formation free energies as a function of temperature by using the harmonic approximation.

To build the dynamical matrix, to obtain the vibrational free energy contribution, one used phonopy to generate the displacements for nearest/next-nearest neighbours to the defect, as the local atomic environment of atoms past the second-nearest shells would have hardly changed from the perfect lattice. From this vibrational frequencies were used to obtain the full free energy of binding of the defect as a function of temperature.

It would be interesting to see how the quasi-harmonic approximation would change improve the accuracy of temperature/concentration predictions with the addition of the change in the lattice parameter with temperature.

5 Gamma surfaces

Energies are accurate to within 2 mJm⁻², comparing the energies of points in the corners which (the zeros of energy). So surface energies might be ± 2 mJm⁻² off which is reasonable.

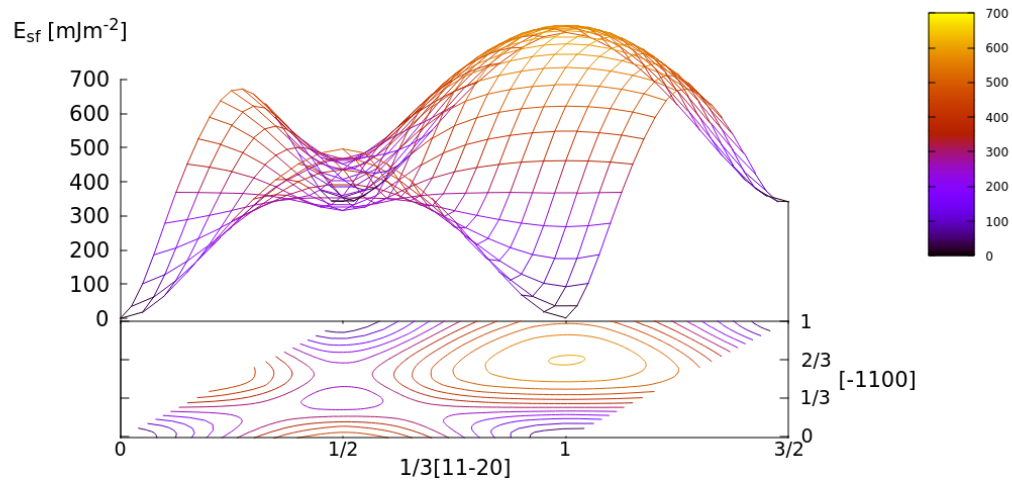
These calculations were done in tight binding with 15 layers for both basal and prismatic. The k-points for the prismatic gamma surfaces were, and for basal they were. DFT comparisons are using results of Rodney.

The Pyramidal surface was obtained using the same 32 atom cell that Ready used in his paper on the pyramidal gamma surface with DFT pseudopotentials.

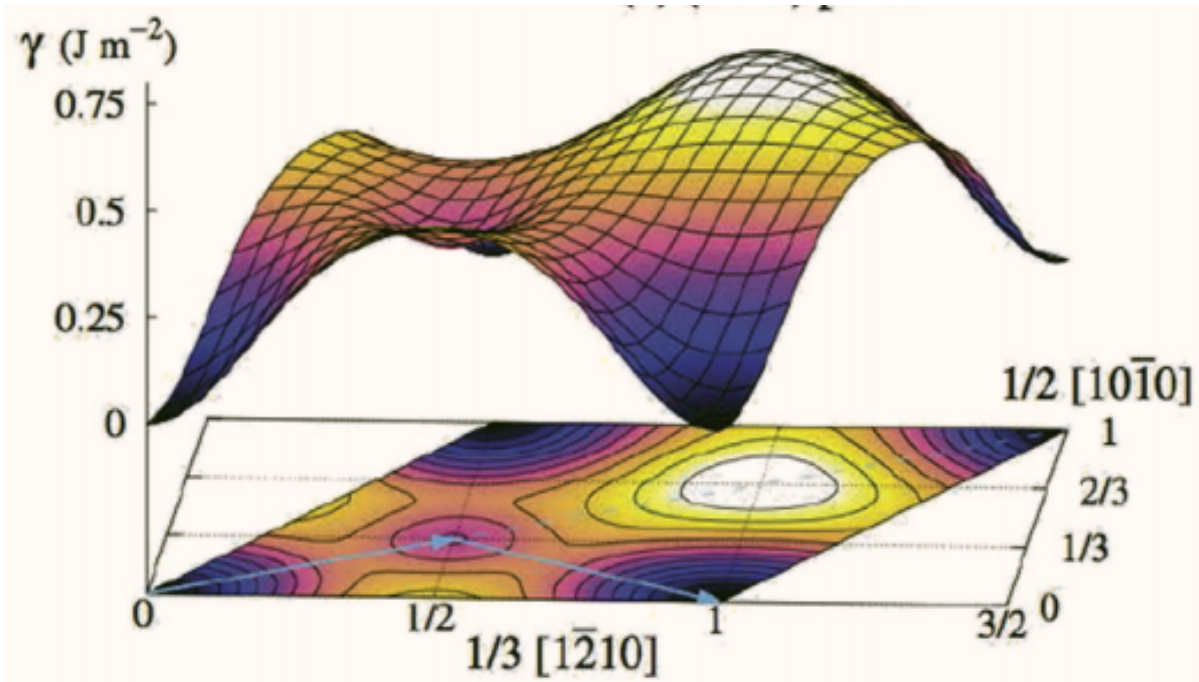
Stacking Fault	Energy [mJm ⁻²]
Prismatic	
Basal I_2	
Basal	
Pyramidal I	

5.1 Basal

TBE:

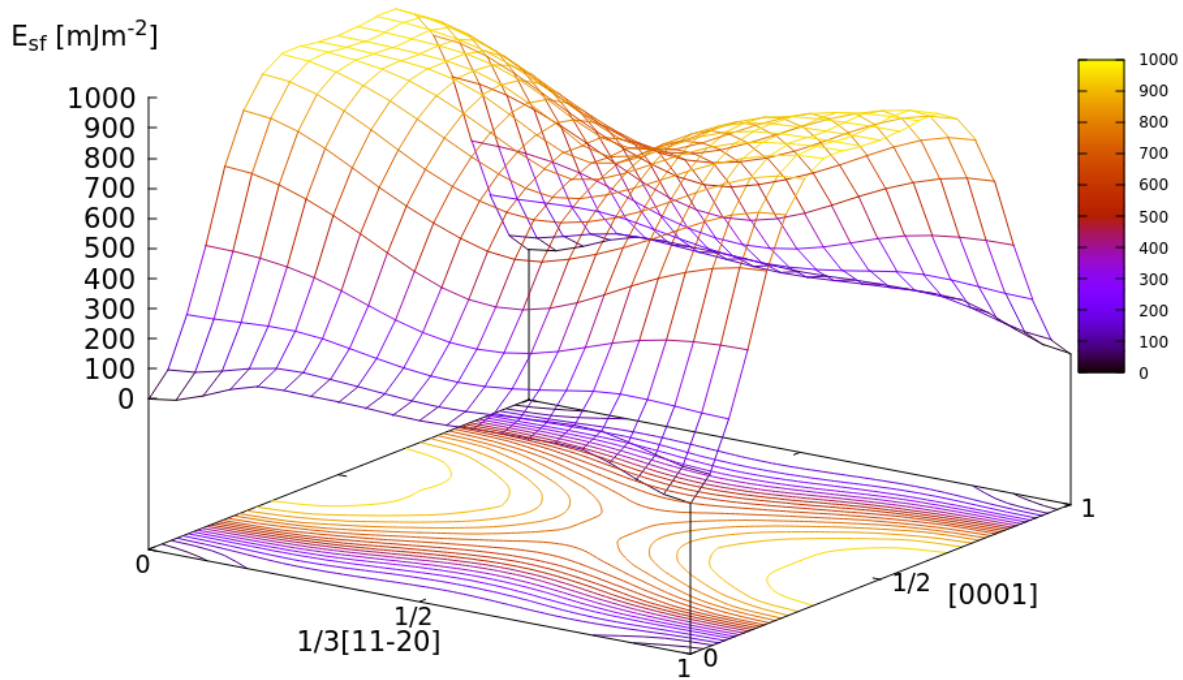


DFT:

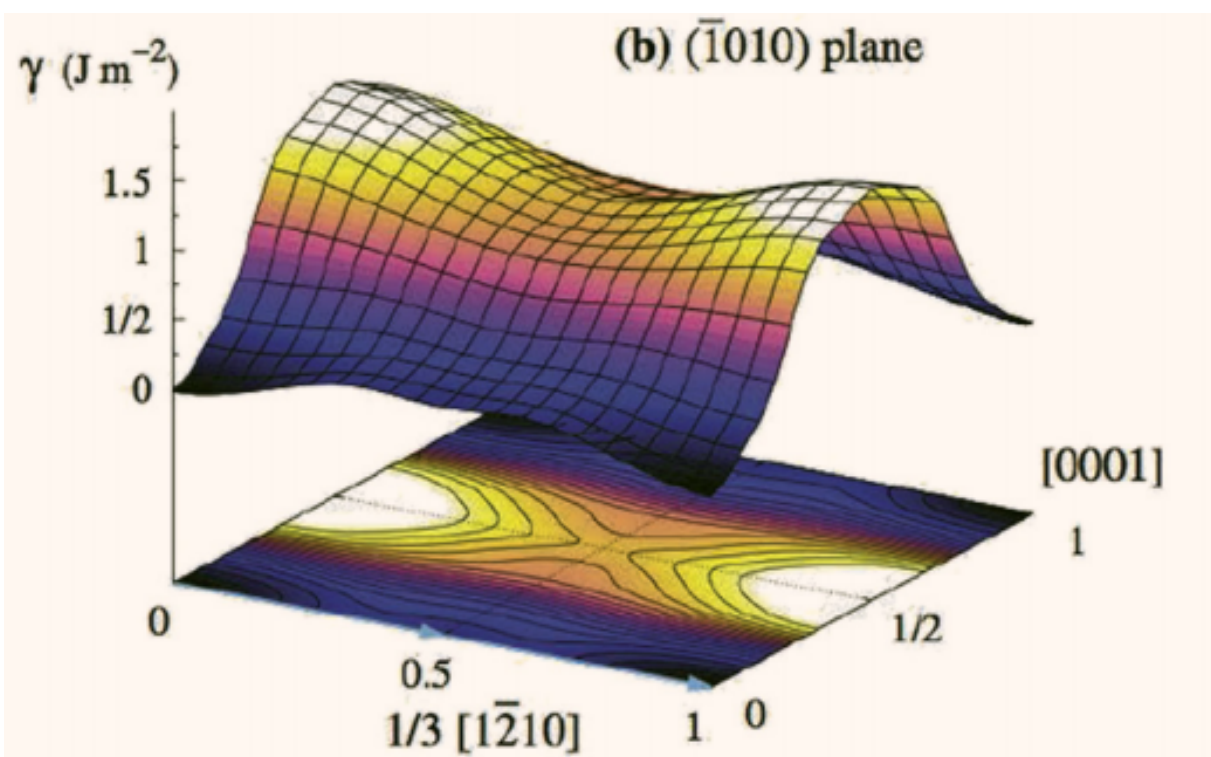


5.2 Prismatic

TBE:

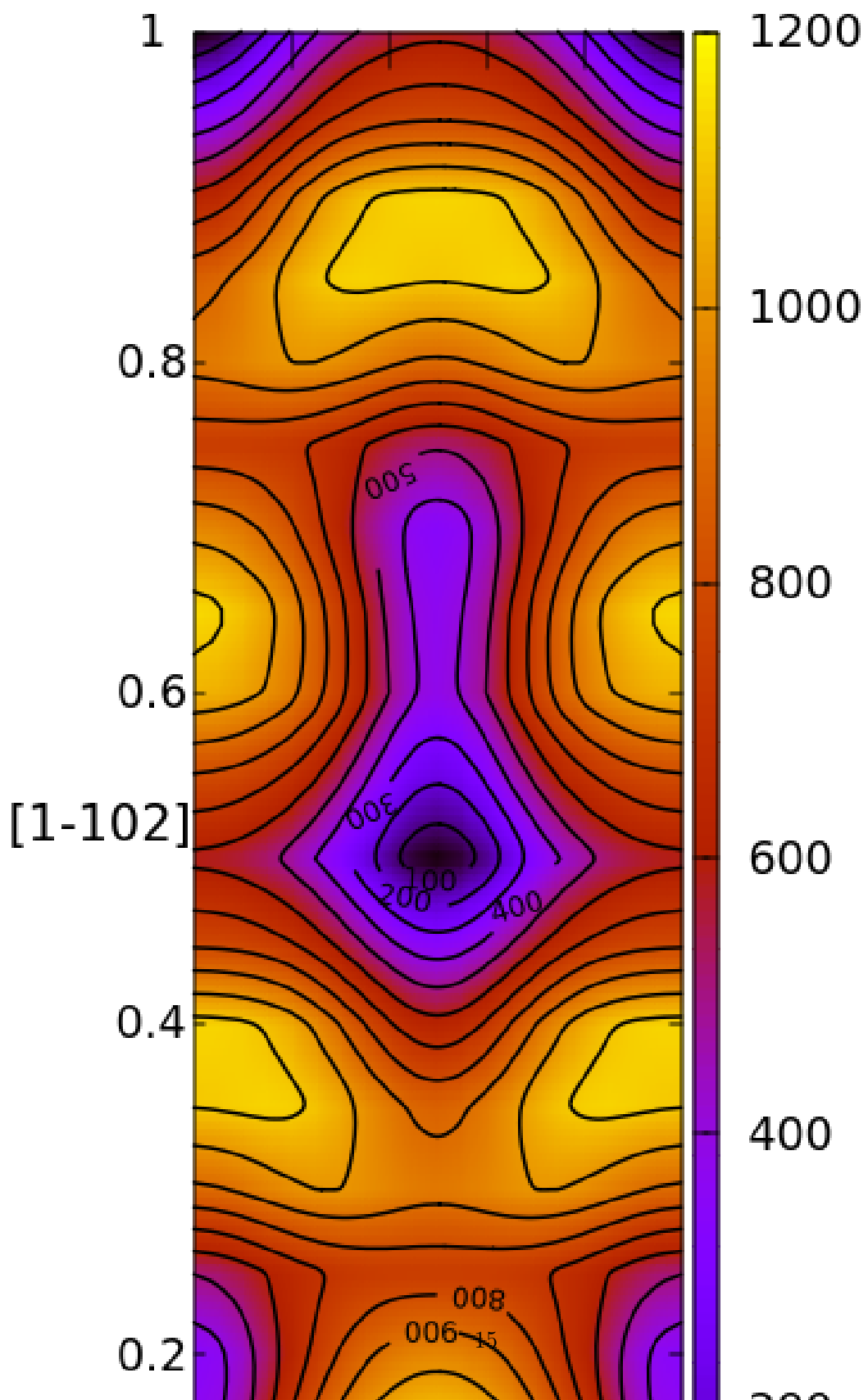


DFT:

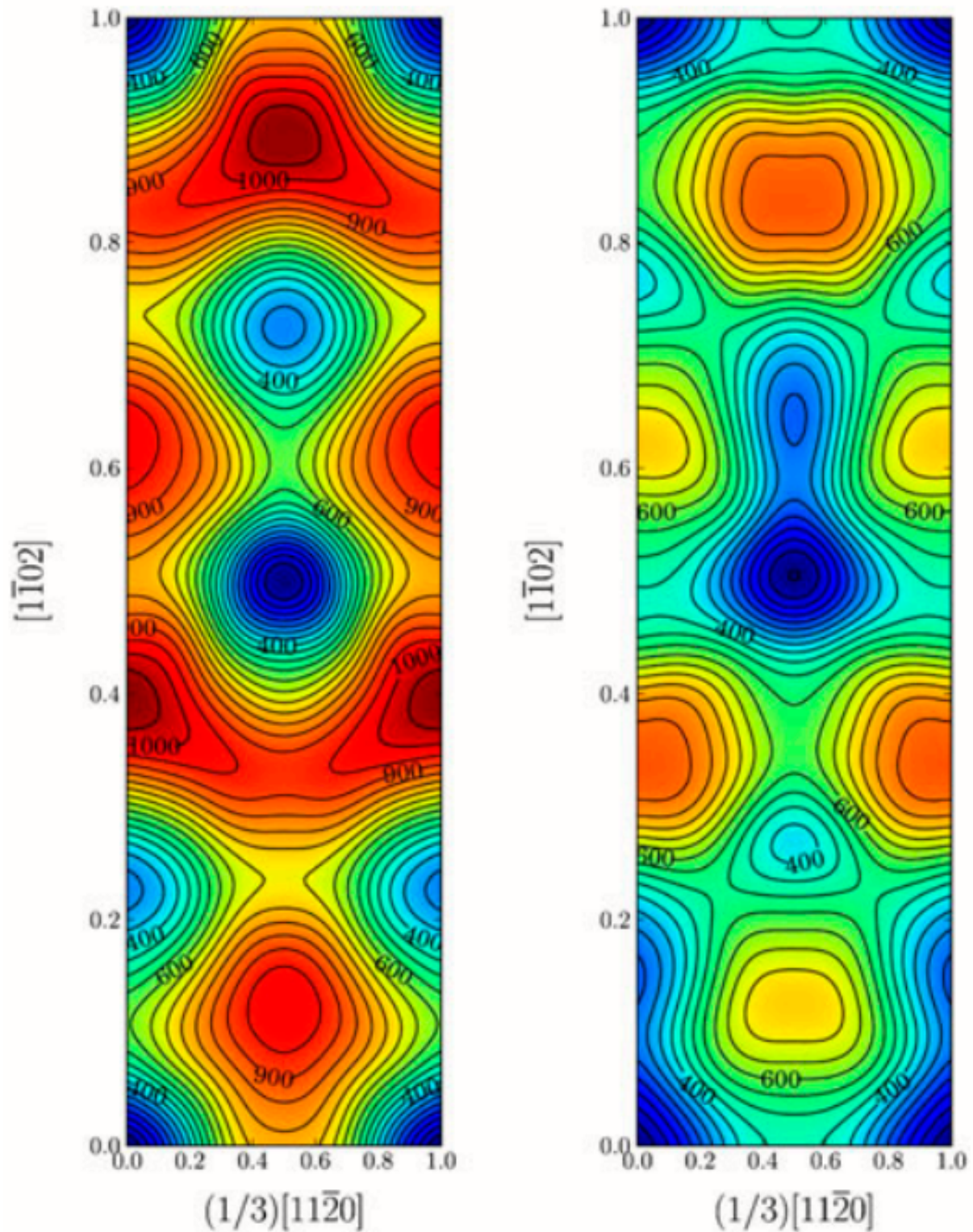


5.3 Pyramidal first order

TBE:



DFT pseudopot:



5.4 Data

basal_{gsdata} prismatic_{gsdata} pyramidal_{gsdata}

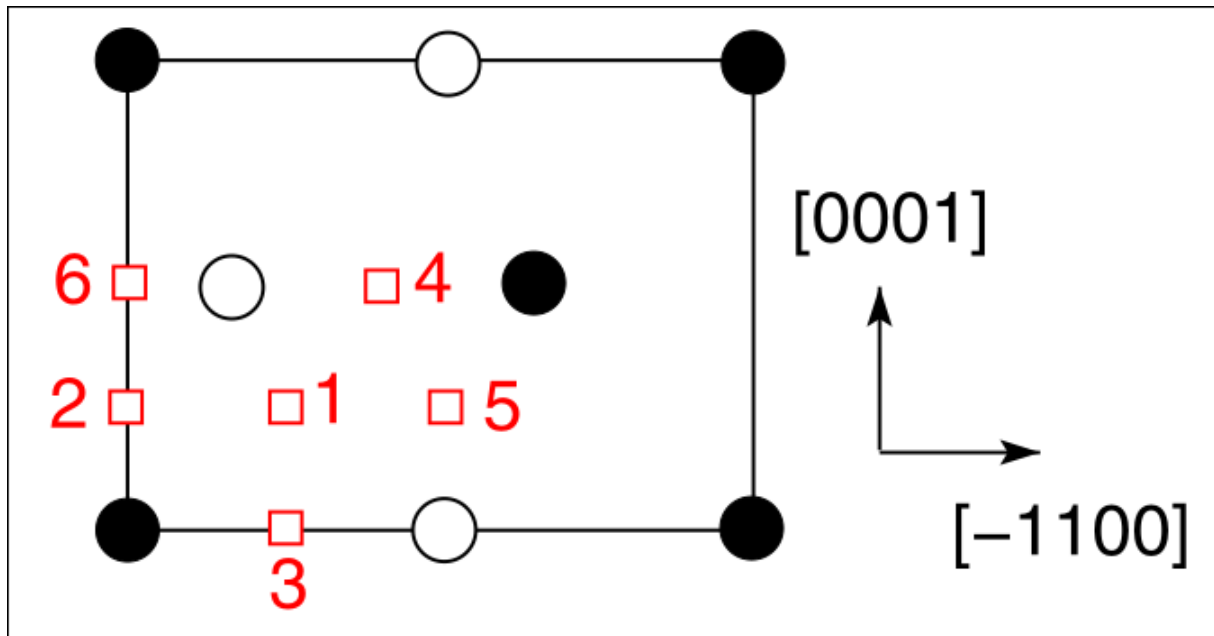
6 Dislocation core structures

6.1 Quadrupolar Array

6.1.1 Methodology

In the following, we see results of dislocation relaxation. The partial differential displacement maps are of dislocations in their initial and final states in different initial positions. The burger's vector seen in these plots is the partial $1/6[11\bar{2}0]$. The original dislocation, of burger's vector $1/3[11\bar{2}0]$, should dissociate into two dislocations on the prismatic plane, each with burger's vector $1/6[11\bar{2}0]$. The atoms were relaxed until the root-mean square force acting on each atom was less than 4×10^{-5} Ryd/Bohr.

These relaxations can be distinguished by the different initial positions of the dislocation centre (elastic centre) as following the paper by Tarrat [1]. Cell geometry was $16 \times 16 \times 1$, where the unit cell was of four atoms, with x , y and z axes given by $[0001]$, $[\bar{1}100]$ and $1/3[11\bar{2}0]$ respectively.



A quadrupolar array of dislocations was created using the "S" arrangement of Clouet [2]: the cut plane of the dislocation dipole is aligned along the diagonal of the cell; dislocations of the same helicity are found on the same x and y planes. This was found to give more satisfactory results for Peierls barrier calculations (the "O" configuration—where the dipole cut plane is parallel to the x axis—resulted in the peierls barrier increasing with cell size, whereas the opposite was found for the "S" arrangement). Displacements for each of the dislocations were determined by solutions to the anisotropic elasticity equations.

To accomodate for the plastic strain introduced with the addition of a dislocation dipole in the simulation cell, an elastic strain was applied, resulting in the tilting of the principal lattice vectors.

To satisfy periodic boundary conditions, periodic displacements were calculated from the superposition of displacements from a 30×30 array of dislocation dipoles, with the subtraction of the spurious linear term due to the conditional convergence of the sum [3].

6.1.2 Discussion

One can see that all of the dislocations have dissociated on the prismatic plane. But there is a difference between initial positions as to upon which prismatic plane they dissociate on, from the original.

None of these states have dissociated onto the proposed pyramidal spread ground state that is proposed by Clouet [4].

Only initial position 2 actually dissociated on a different prismatic plane to the others.

The positions of the partials are also different once each of the separate initial positions have been relaxed.

IP2 and IP3, although they are on different planes, have a very similar core structure to each other. They are both asymmetric cores.

IP1 has the upper partial dislocation located within an adjacent triangle to the left, compared to IP2 and IP3. The lower partial has been shifted downwards, by one triangle down and to the right, with respect to IP3. The core structure of IP5 is indistinguishable from IP1. These cores can be deemed as metastable, as they have a slightly higher energy than the other cores.

The upper partial of IP4 has been displaced upwards by one Peierls valley with respect to IP3. The lower partial is in the same triangle as IP3. IP4 is a mirrored core.

Each of these cores are asymmetric, using the definition by Tarrat [1].

The energies for each of the dislocation cores, when relaxed to 1×10^{-5} Ryd Bohr is

Initial position	E_{total} [Ryd]
1	-331.54658899
2	-331.54660063
3	-331.54660053
4	-331.54660061
5	-331.54658717

The dissociation distance is consistent between the different initial positions of the elastic centres. The distance is $\approx 4c = 35.4$ Bohr = 18.7, this is double the distance seen in Ghazisaedi and Trinkle [5] and double the distance that is found in the DFT Zr results by Clouet [2].

6.1.3 TODO Dissociation Distance Analysis

Following [2], one can use dislocation elasticity theory to compute the dissociation distance of a dislocation in both the basal and prism planes. The energy variation caused by a dissociation length d is

$$\Delta E_{\text{diss}}(d) = -b_i^{(1)} K_{ij} b_j^{(2)} \ln\left(\frac{d}{r_c}\right) + \gamma d,$$

where $\mathbf{b}^{(i)}$ are the Burger's vectors of the dissociated dislocations. γ is the corresponding gamma surface energy and K is the Stroh matrix. Controlling the dislocation core radius and the dislocation elastic energy, one can find the equilibrium dissociation distance as

$$d^{\text{eq}} = \frac{b_i^{(1)} K_{ij} b_j^{(2)}}{\gamma}$$

With the orientation of the simulation cell as, $U_1 = na\frac{1}{2}[10\bar{1}0]$, $U_2 = mc[0001]$, $U_3 = a\frac{1}{3}[1\bar{2}10]$, one finds the components of the Stroh matrix as:

$$K_{11} = \frac{1}{2\pi} (\bar{C}_{11} + C_{13}) \sqrt{\frac{C_{44}(\bar{C}_{11} - C_{13})}{C_{33}(\bar{C}_{11} + C_{13} + 2C_{44})}} \quad (1)$$

$$K_{22} = \sqrt{\frac{C_{33}}{C_{11}}} K_{11} \quad (2)$$

$$K_{33} = \frac{1}{2\pi} \sqrt{\frac{1}{2} C_{44}(C_{11} - C_{12})} \quad (3)$$

here, $\bar{C}_{11} = \sqrt{C_{11}C_{33}}$.

From the gamma surface, for the basal plane one expects a dissociation of $1/3[1\bar{2}10] = 1/3[1\bar{1}00] + 1/3[0\bar{1}10]$. Then dissociation length in the basal plane is given by

$$d_b^{\text{eq}} = \frac{(3K_{33} - K_{11})a^2}{12\gamma_b}$$

For the prism plane the $1/3[1\bar{2}10]$ dislocation can dissociate into $1/6[1\bar{2}10] \pm \alpha(c/a)[0001]$ where the parameter α controls the position of the stacking fault minimum along the [0001] direction. Only in interatomic potentials like the EAM, do we find that $\alpha = 0.14$.

The dissociation length is

$$d_p^{\text{eq}} = \frac{(K_{33}a^2 - 4\alpha^2 K_{22}c^2)}{4\gamma_p}$$

1. Analysis with Final Ti model.

$$d_p^{\text{eq}} = \frac{(K_{33}a^2 - 4\alpha^2 K_{22}c^2)}{4\gamma_p}$$

Using the above equation to calculate the dissociation distance with $K_{33} = 6.79853 \text{ GPa} = 6.79853/160.21766208 \text{ eV}/\text{\AA}^3 = 0.042433087 \text{ eV}/\text{\AA}^3$, $\alpha = 0$ and $\gamma_p = 98.95340236 \text{ mJm}^{-2} = 1.6021766208 * 10^{-19} * 10^{-3} * 10^{20} * 98.95340236 \text{ eV}/\text{\AA}^3 \$ = 1.58540827809\$ \text{ eV}/\text{\AA}^3$, $a = 2.955577$ we have the equilibrium dissociation distance in the prismatic plane as $d_p^{\text{eq}} = 0.05845 \text{ \AA}$, which seems very small, comparing to the differential displacement maps...

Further scrutiny is necessary.

6.1.4 TODO Disregistry Analysis

Look into the theory of dissociation distance in Clouet paper [2]

Disregistry given by the Peierls-Nabarro model. Analytic expression given in Hirth and Lothe [6].

Disregistry $D(x)$ is defined as the displacement difference between the atoms in the plane just above and those just below the dislocation glide plane. The derivative of this function $\rho(x) = \partial D/\partial x$ corresponds to the dislocation density.

$$D_{\text{dislo}} = \frac{b}{2\pi} \left\{ \arctan \left[\frac{x - x_0 - d/2}{\zeta} \right] + \arctan \left[\frac{x - x_0 + d/2}{\zeta} + \frac{\pi}{2} \right] \right\}$$

Given x_0 is the dislocation position, d is dissociation length and ζ is the spreading of each partial dislocation.

$$\begin{aligned} D_L &= \sum_{n=-\infty}^{\infty} D_{\text{dislo}}(x - nL) \\ &= \frac{b}{2\pi} \left\{ \arctan \left[\frac{\tan \left(\frac{\pi}{L} [x - x_0 - d/2] \right)}{\tanh \left(\frac{\pi\zeta}{L} \right)} \right] + \pi \left[\frac{x - x_0 - d/2}{\zeta} + \frac{1}{2} \right] \right. \\ &\quad \left. + \arctan \left[\frac{\tan \left(\frac{\pi}{L} [x - x_0 + d/2] \right)}{\tanh \left(\frac{\pi\zeta}{L} \right)} \right] + \pi \left[\frac{x - x_0 + d/2}{\zeta} + \frac{1}{2} \right] \right\}, \end{aligned}$$

where $\lfloor \cdot \rfloor$ is the floor function.

For an array of dislocations in the S arrangement, $D(x) = D_L(x)$, with $L = mc$, where m is the number of repeated unit cells in the U_2 direction.

Here, $U_1 = na\frac{1}{2}[10\bar{1}0]$, $U_2 = mc[0001]$, $U_3 = a\frac{1}{3}[1\bar{2}10]$.

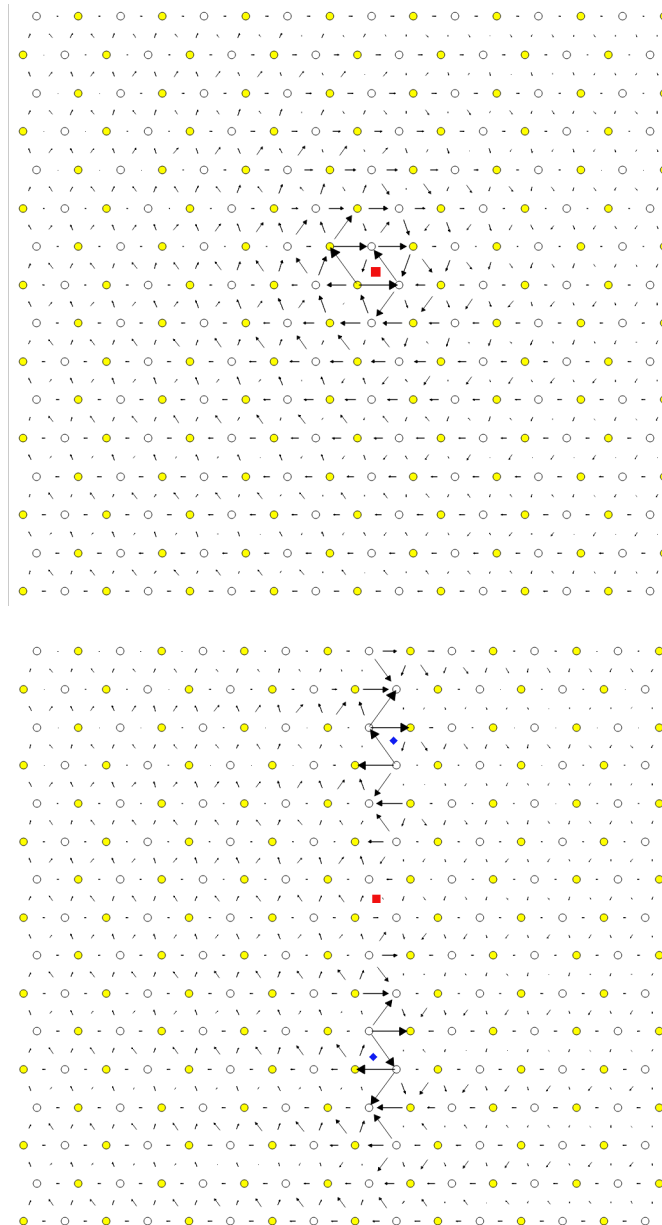
Therefore, using this, one can fit the three fitting parameters: the dislocation position x_0 , the dissociation length d , and the spreading ζ . This procedure allows us to determine the location of the dislocation center.

From the Peierls-Nabarro model of an edge dislocation, one finds that the displacement in x $u_x = -\frac{b}{2\pi} \tan^{-1} \frac{x}{\zeta}$, where $\zeta = d/2(1 - \nu)$, where the width of the dislocation is 2ζ , where the disregistry is one-half the maximum value at $x=0$.

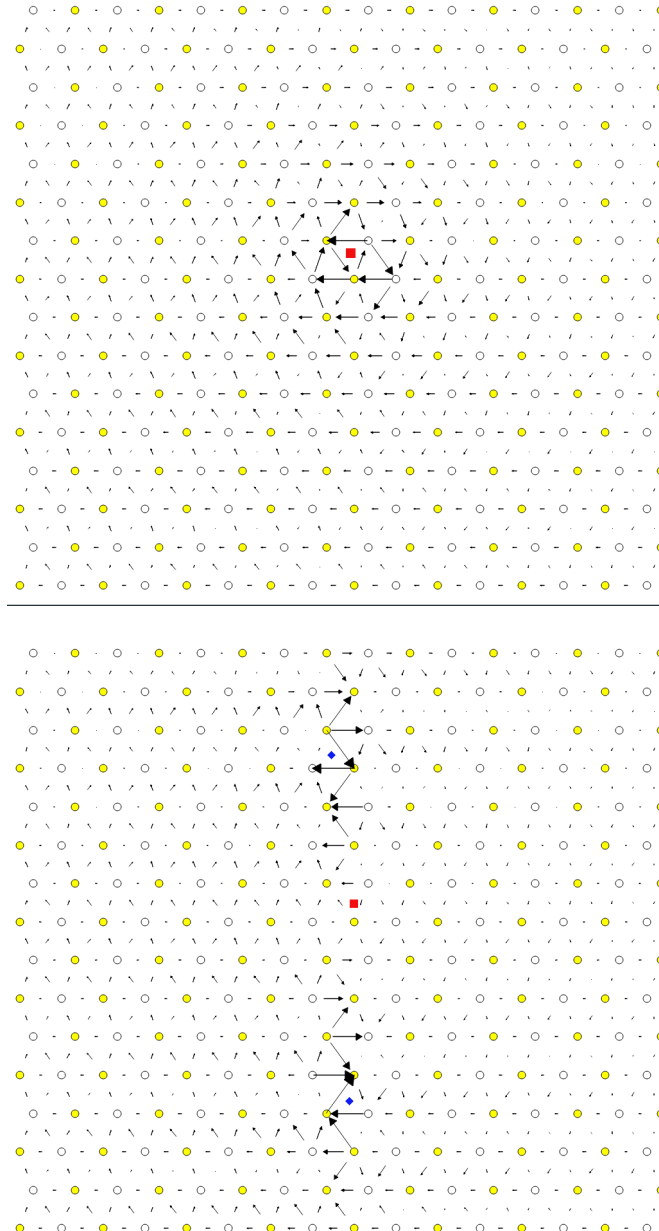
For a screw dislocation, one essentially replaces ζ with $\eta = (1 - \nu)\zeta = d/2$

For all interaction models, we find that this center lies in between two (0001) atomic planes. One can see in Fig. 6 of [2] that this position corresponds to a local symmetry axis of the differential displacement map. This is different from the result obtained by Ghazisaeidi and Trinkle [5] in Ti where the center of the screw dislocation was found to lie exactly in one (0001) atomic plane.

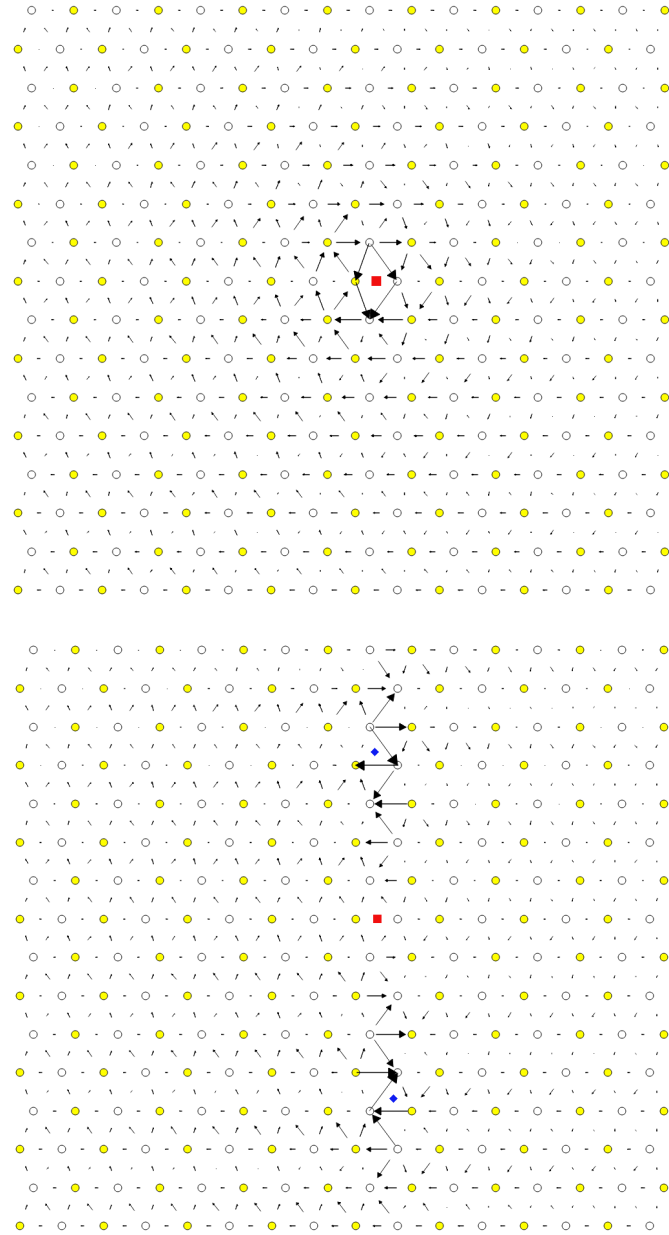
6.1.5 IP1



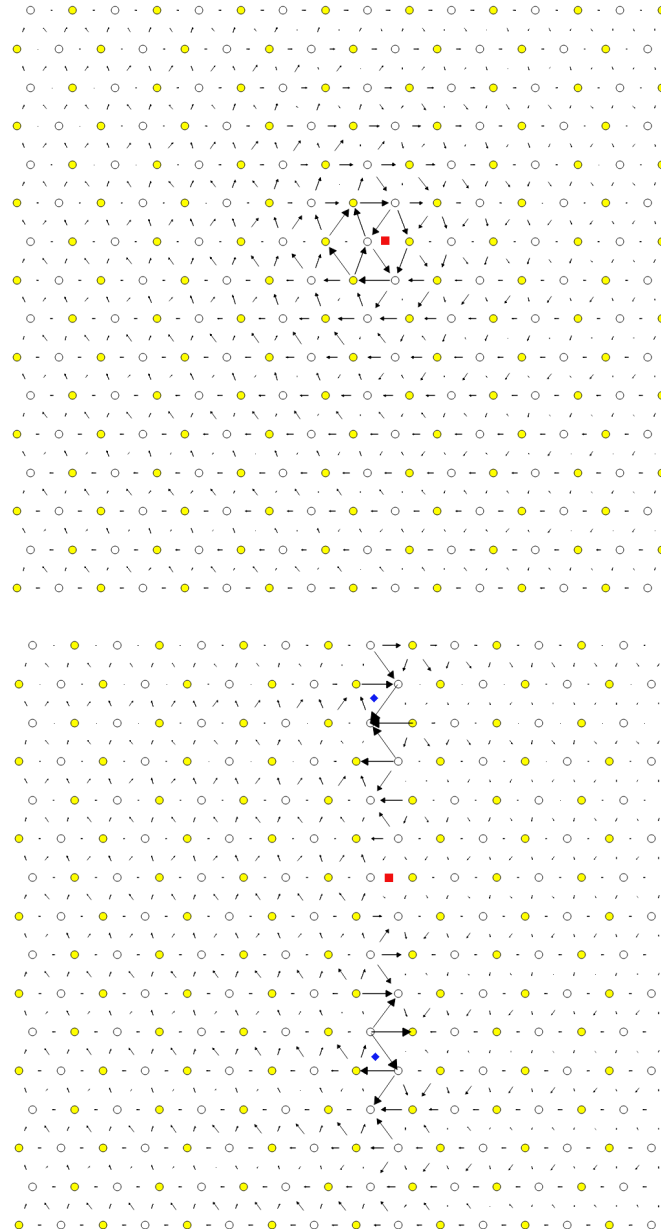
6.1.6 IP2



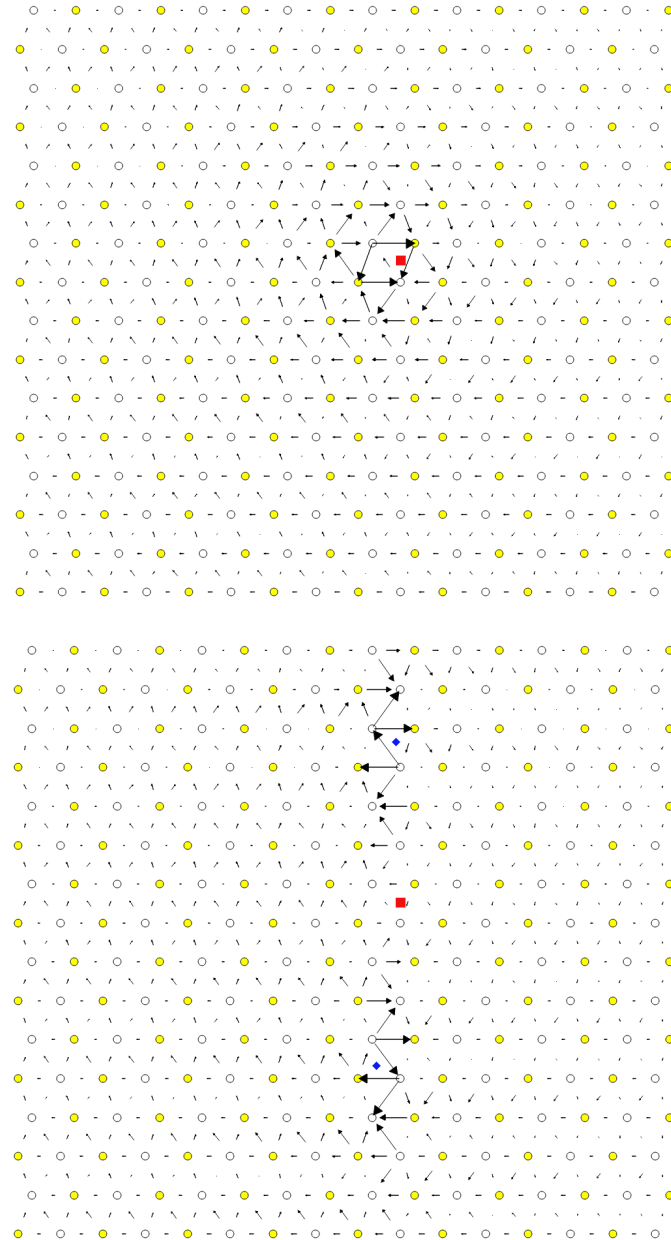
6.1.7 IP3



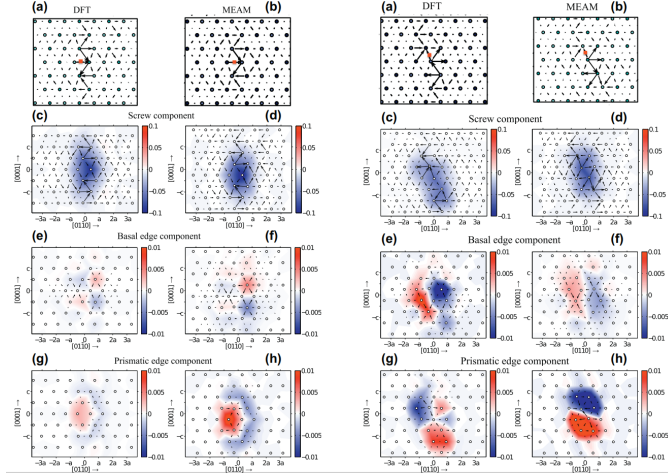
6.1.8 IP4



6.1.9 IP5



6.1.10 Ghazisaeidi Results for comparison



6.1.11 TODO Replot all dislocations and do analysis in Atomman.

This will be very useful as one can see plots of the Nye tensor, so one can truly see where the partials are and their dislocation centres.

6.1.12 Peierls Stress

By straining the cell of a relaxed lattice and incrementally increasing the strain, one can find the minimum stress necessary to move a dislocation from one Peierls valley to the next.

1. Applying strain

Applying strain as in [7].

Here we are incrementing the strain by $0.001C^{\text{rot}}$, where C^{rot} is the transformed elastic constant necessary for transforming a strain into a stress from the relation $\sigma_{ij} = C_{ijkl}\varepsilon_{kl}$.

The original elastic constant matrix in its untransformed state is:

$$C = \begin{bmatrix} 171.6093 & 94.6594 & 61.2262 & 0. & 0. & 0. \\ 94.6594 & 171.6093 & 61.2262 & 0. & 0. & 0. \\ 61.2262 & 61.2262 & 198.9006 & 0. & 0. & 0. \\ 0. & 0. & 0. & 47.4255 & 0. & 0. \\ 0. & 0. & 0. & 0. & 47.4255 & 0. \\ 0. & 0. & 0. & 0. & 0. & 38.4749 \end{bmatrix}$$

Transforming it into the dislocation coordinate system, by the rotation

$$R = \begin{bmatrix} 1 & 0 & 0 \\ 0 & 0 & -1 \\ 0 & 1 & 0 \end{bmatrix}$$

$$C^{\text{rot}} = \begin{bmatrix} 171.6093 & 61.2262 & 94.6594 & 0. & 0. & 0. \\ 61.2262 & 198.9006 & 61.2262 & 0. & 0. & 0. \\ 94.6594 & 61.2262 & 171.6093 & 0. & 0. & 0. \\ 0. & 0. & 0. & 47.4255 & 0. & 0. \\ 0. & 0. & 0. & 0. & 38.4749 & 0. \\ 0. & 0. & 0. & 0. & 0. & 47.4255 \end{bmatrix}$$

For finding the Peierls stress to move partials away from each other on the prismatic plane one finds that the stress if given by $\sigma_{xy} = \sigma_{12} = 2C_{66}^{\text{rot}}\varepsilon_{12}$, where $C_{66}^{\text{rot}} = 47.4255$ GPa.

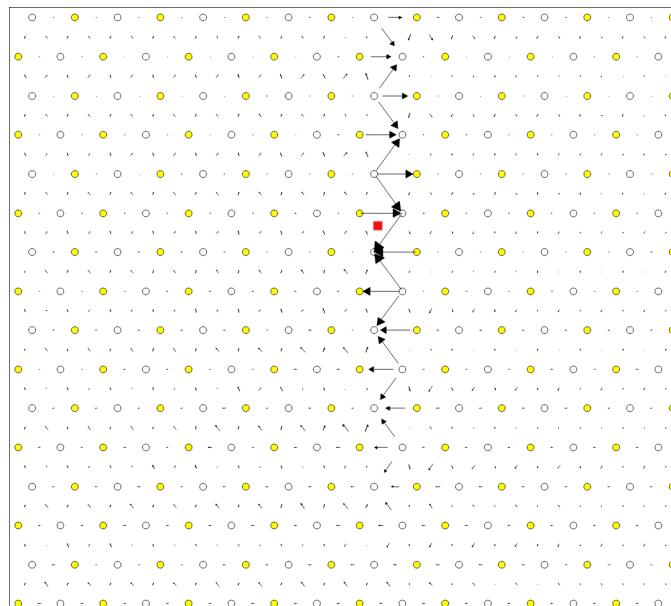
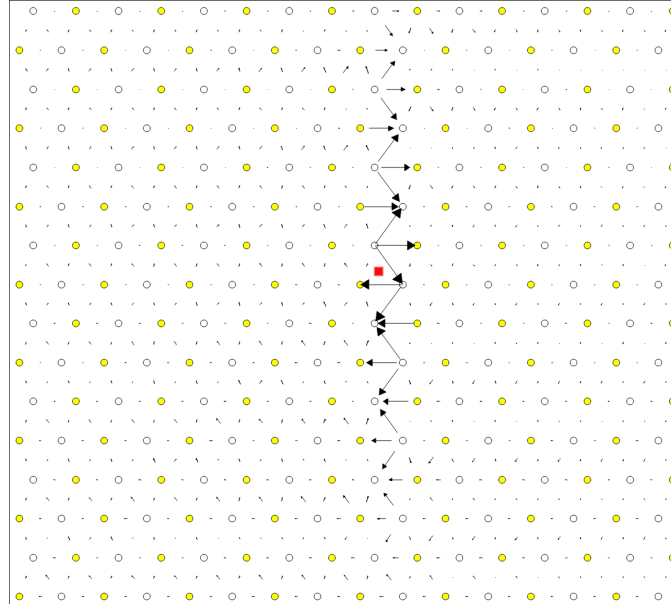
To move the whole dislocation on the prismatic plane, one needs a stress applied which is $\sigma_{xz} = \sigma_{13} = 2C_{55}^{\text{rot}}\varepsilon_{13}$, $C_{55}^{\text{rot}} = 38.4749$ GPa.

To move the dislocation onto the basal plane one needs to apply as stress given by $\sigma_{yz} = \sigma_{23} = 2C_{44}^{\text{rot}}\varepsilon_{23}$, $C_{44}^{\text{rot}} = 47.4255$ GPa.

2. xz Strain

Applying an xz strain to the lattice causes the dislocation to move along the prismatic plane.

Using an increment in the strain of $1 \times 10^{-4}C^*$, where C^* is the transformed elastic constant, with a value of $C_{44}^* = 38.4749$ GPa, we find that the dislocation moves from one Peierls valley along the prismatic plane at $0.0012C_{44}^*$, giving a Peierls stress of $\sigma_{xz} = 2C_{44}\varepsilon_{xz} = 0.0923$ GPa



3. yz Strain

This is the strain necessary for movement on the basal plane. Following the procedure above, one does not obtain recombination of partials, or any movement of the dislocation onto the basal plane. Increasing the accumulated strain up to $10\backslash 0.001C$ to see if there is any difference.

Furthermore, one is starting from initial anisotropic elasticity solutions, applying strain and then relaxing, such that one may be able to find a strain where the screw dislocation has spread in the basal plane.

4. xy strain

An xy strain can move the partials of the prismatic plane apart.

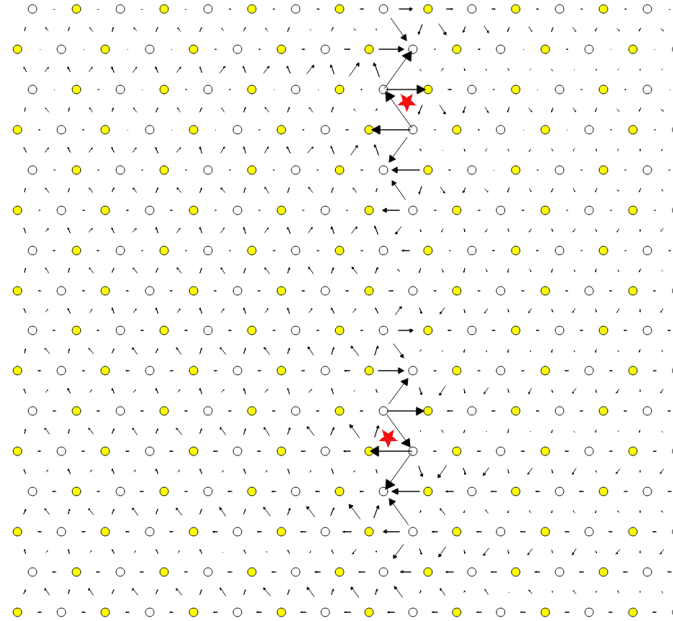
One can find the Peierls stress for these single partials to move in opposite directions.

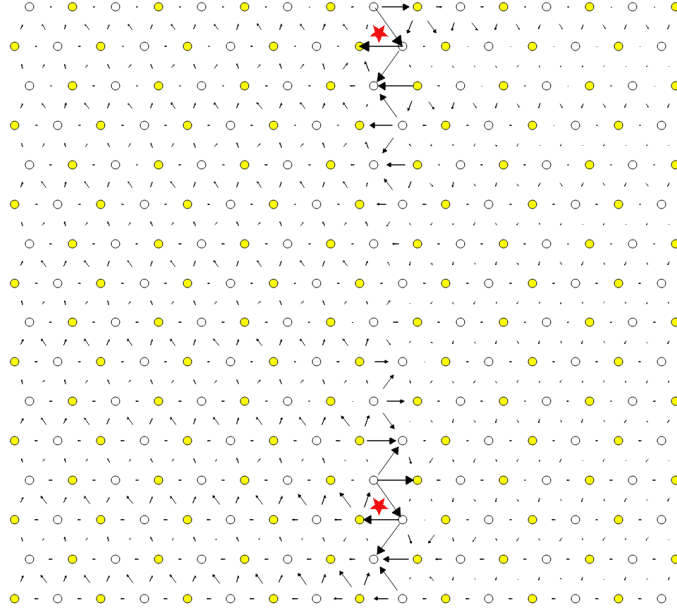
Here the α parameter is 0.03.

This means that the stress necessary to move the partial dislocations apart is

$$\begin{aligned}\sigma_{12} &= C_{1212}\varepsilon_{12} \\ &= 2C_{66}^{\text{Voigt}}\varepsilon_6^{\text{Voigt}} \\ &= (C_{11} - C_{12})\varepsilon_6^{\text{Voigt}} \\ &= 47.4255 \times 0.03 \\ &= 1.42 \text{ GPa}\end{aligned}$$

The strain is applied to the whole cell, as the dislocation cell is periodic, then the stress upon each partial is the same.





5. Pyramidal Strain

For a strain to transform the dislocation into the metastable, pyramidal state, one can apply a strain which applies shear to the dislocation whereby the maximum resolved shear stress is on the first-order pyramidal plane.

In the coordinate system of the dislocation, one can estimate the strain necessary by the ratio of stresses for the basal and prismatic planes. The proportions strains σ_{xz} and σ_{yz} should be $c/a : \sqrt{3}/2 \approx 1.83 : 1 \approx 1 : 0.54683$.

Unfortunately, this proportion does not work, nor does the ratio $\sigma_{xz} : \sigma_{yz} \approx 1 : 1/10$. A much, much lower proportion of the strain is necessary as the dislocation just moves prismatically. Once one finds the Peierls stress for the basal plane, we can estimate a more realistic proportion.

6.1.13 Data

IP1 IP2 IP3 IP4 IP5

6.1.14 Directory of the results

```
file:///home/tigany/Documents/ti/2019-09-11_final_model/tbe/dislocations/2019-11-08_no_omega_ordering_ec_latpar/ file:///home/tigany/Documents/ti/final_model_2019-11
```

6.2 Cluster Method

6.2.1 Methodology

This section comprises the results of using the cluster method to simulate single dislocations in the Ti model.

The cluster method simulates dislocations by only imposing periodicity in the direction of the dislocation line (the z-axis, in this case). This is the advantage over dislocation dipole simulations as there are no dislocation-dislocation interactions which interfere with relaxation, but in their stead, there are dislocation-boundary interactions, which inhibit the relaxation of the dislocation core.

As the number of atoms in a cluster increases, the resulting core structure upon relaxation will tend to the bulk core structure, as there is a reduction in the spurious dislocation-surface interaction. Due to the finite size of simulations, the geometry of the cell is important. With sufficient cell size, dislocation core

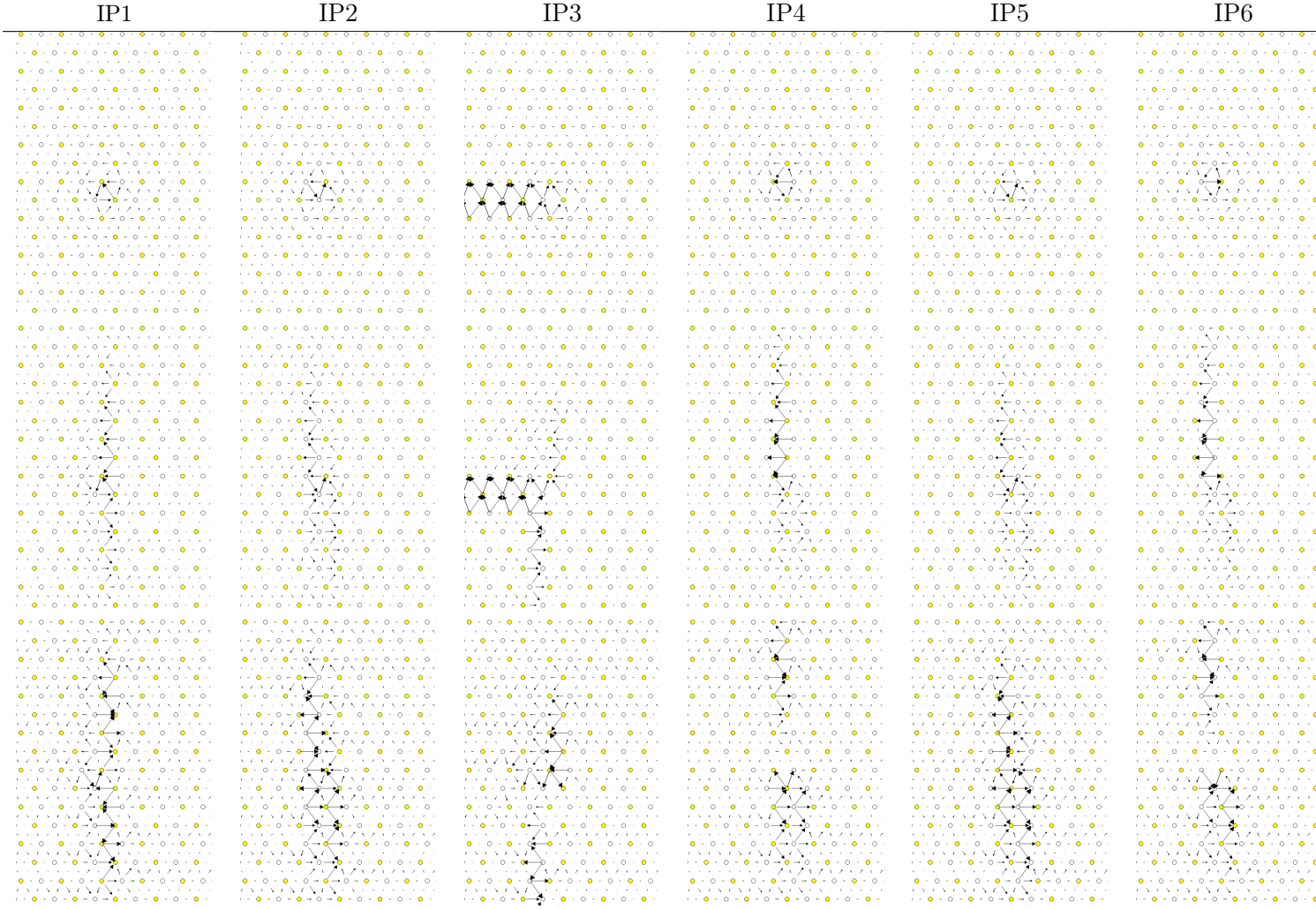


Table 1: Differential displacement map of dislocation relaxations in different initial positions in a cylindrical cell. Row 1: Prior to relaxation, $\mathbf{b} = 1/3\langle 1\bar{2}10 \rangle$. Row 2: After relaxation, $\mathbf{b} = 1/3\langle 1\bar{2}10 \rangle$. Row 3: After relaxation, $\mathbf{b} = 1/6\langle 1\bar{2}10 \rangle$

structure should be invariant to the boundary conditions imposed. To ascertain how sensitive the new Ti model is to boundary conditions, two different cell geometries were used: circular and hexagonal. Each of these had two layers of fixed (inert) atoms around a dynamic central region.

All relaxations were carried out using the Fletcher-Powell conjugate gradient algorithm with a force tolerance of 4×10^{-5} Ryd/Bohr $\approx 1 \times 10^{-3}$ eV/, with a k-point mesh of 1x1x30.

Tarrat [1] deemed that the use of hexagonal cluster cell geometries were more beneficial to determine the core structure of dislocations due to a lower total surface energy, implying a reduction in the magnitude of dislocation-surface interaction.

6.2.2 Circular Cluster

6.2.3 Hexagonal Cluster

6.2.4 Peierls Stress

1. yz strain (basal transformation)

In the cluster method, by incrementally increasing the strain in increments of 0.001, one found at

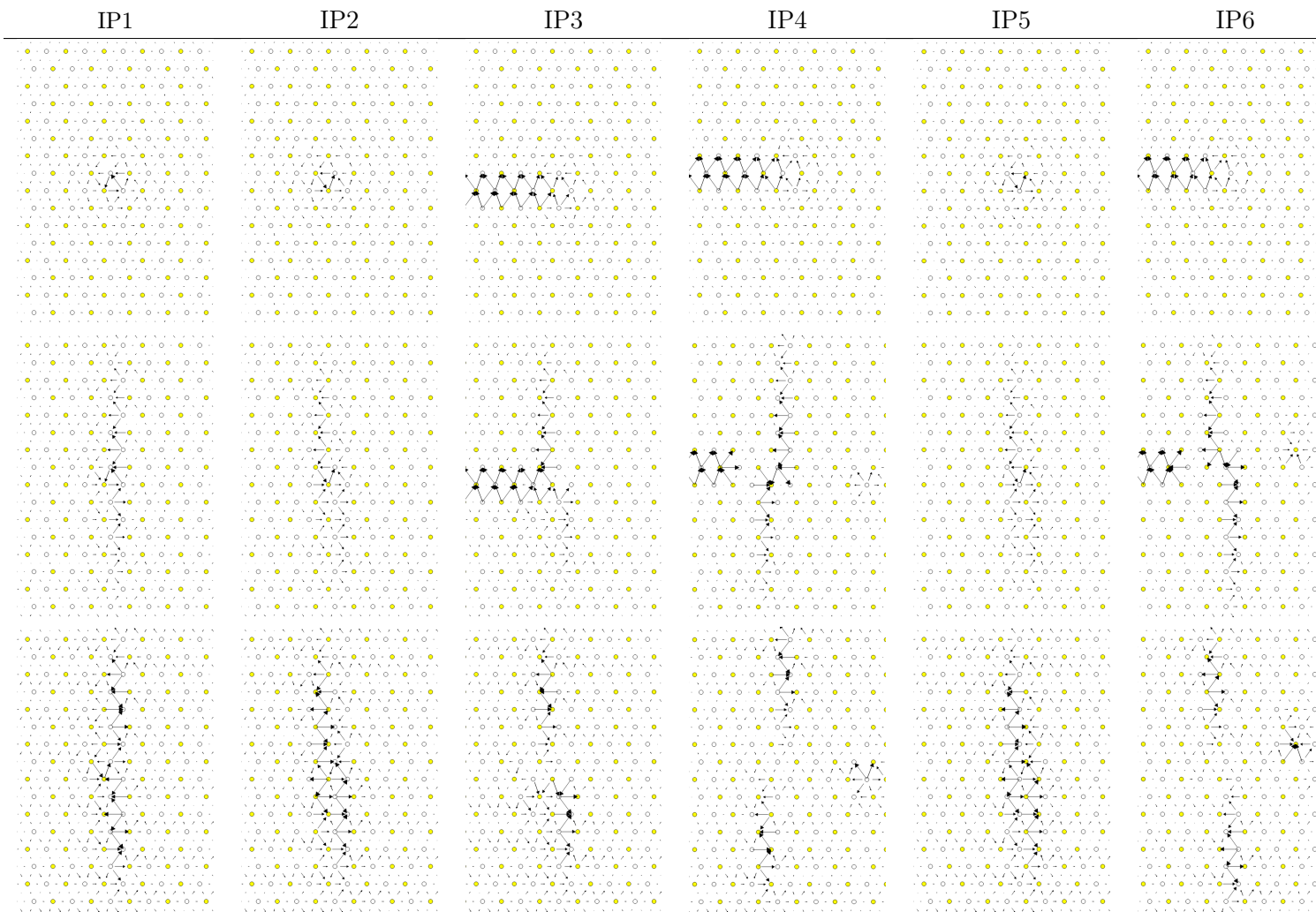


Table 2: Differential displacement map of dislocation relaxations in different initial positions in a hexagonal cell. Row 1: Prior to relaxation, $\mathbf{b} = 1/3\langle 1\bar{2}10 \rangle$. Row 2: After relaxation, $\mathbf{b} = 1/3\langle 1\bar{2}10 \rangle$. Row 3: After relaxation, $\mathbf{b} = 1/6\langle 1\bar{2}10 \rangle$

0.035 in the IP4 configuration, that the bottom partial dislocation suddenly splits away from the prismatic plane the dislocation was spread on.

The dislocations are then of basal character (the partial left on the prismatic plane being $1/3\langle 0\bar{1}10 \rangle$, with the other partial being $1/3\langle 1\bar{1}00 \rangle$).

This lower partial moved to the right by 6 lattice parameters and down by 1 clat. There is an I2 (fcc) stacking fault which separates the prismatic plane from the partial. The core structure is only basally spread upon movement. The other partial moves down the prismatic plane to join the stacking fault to join in a more compact, yet still basally dissociated dislocation. The resultant displacements from the prismatic spreading are removed.

Then after moving across by 1 alat and up 2 clat, the two partials stay dissociated on the basal plane, being separated by 4 alat at a maximum. The fcc stacking fault is subsequently removed by recombination of the dislocations into a compact $1/3\langle 1\bar{2}10 \rangle$ core. This core then begins to spread in two adjacent prismatic planes with a pyramidal core spreading joining the two.

The spreading changes from pyramidal with prismatic on two different prismatic planes, to purely prismatic on the rightmost prismatic plane. Whereupon, after moving upwards, the dislocation spreads in this plane identically to the spreading of an IP4 core configuration upon relaxation.

This means that the Peierls stress for the basal plane, in the case of a cluster calculation is $\sigma_{yz} = \sigma_{23} = 2C_{44}^{\text{rot}}\varepsilon_{23}$, with $\varepsilon = 0.035$, and $C_{44}^{\text{rot}} = 47.4255 \text{ GPa}$, we get $\sigma_{yz}^{\text{crit.}} = 0.035 \times 47.4255 \approx 1.66 \text{ GPa}$.

6.2.5 Discussion

The boundary conditions of the cell seem to be quite important in determining the core structure. There are differences between the core structure of some of the initial positions between the hexagonal and cylindrical cells.

IP1, IP2 and IP5 dislocation centres result in the same core configuration regardless of the geometry of the cell.

7 Binding of oxygen to dislocations

7.1 Quadrupolar Array

Using a relaxed 12×12 slab with an "S" quadrupolar arrangement of dislocations, of which the elastic centres of each are in initial position 5, one can repeat this cell three times in the \$z\$-direction. One can place oxygen in octahedral sites near the dislocation core in the middle layer at varying distances from the core. By repeating this, one can ascertain how the binding energy of oxygen to dislocations changes with distance from the core.

One does not expect a lot of interaction from the dislocation core beyond a few burgers vectors of distance of the solute from the core, as the core field decays rapidly. Beyond this, one would expect resulting in a lot of the binding energy to come from the interaction of the strain fields generated by the oxygen interstitial deforming an octahedral site and the strain field of the dislocation itself.

Oxygen was placed near both cores in the simulation cell, such that the quadrupolar array was more stable.

Oxygen in the closest octahedral sites in the same basal plane of the dislocation, unsurprisingly, produced the most change from the initial dislocation position. Interestingly, it seems that due to the distortion of the octahedral site from the interstitial oxygen, the shear stress field produces is above the Peierls stress necessary for the dislocation to glide on the prismatic plane. This results in the quadrupolar cores moving to form an S configuration of an opposite type.

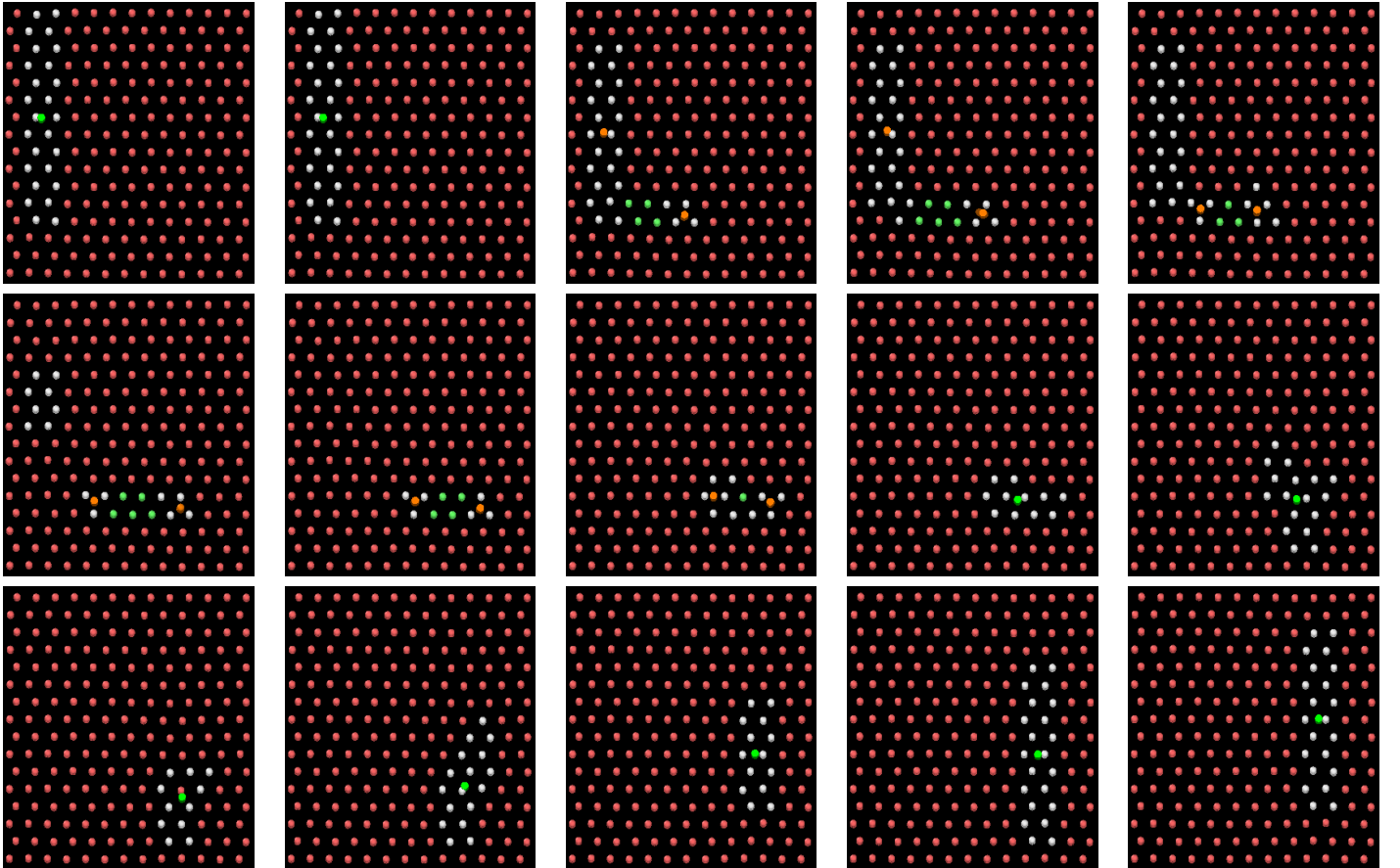


Table 3: Behaviour of $\mathbf{b} = 1/3\langle 1\bar{2}10 \rangle$ screw dislocation (lime green dot) under action of yz strain to force movement on basal plane. White-coloured atoms denote defected areas of the lattice due to the spreading of dislocations/residual displacement. Red-coloured atoms denote a local hcp structure. Green-coloured atoms denote local fcc structure. The dislocation starts out dissociated in prismatic plane. $\sigma_{yz} \approx 1.66$ GPa forces a prismatic partial to move on its basal plane. The other basal partial moves down to meet the same basal plane as the partial which has broken away. These partials are separated by an I2 stacking fault (green coloured atoms). The basally dissociated partials recombine to form a $1/3\langle 1\bar{2}10 \rangle$ screw , whereupon after briefly having a compact core structure, the core spreads in both the pyramidal and prismatic planes, before stabilising in a purely prismatically spread configuration.

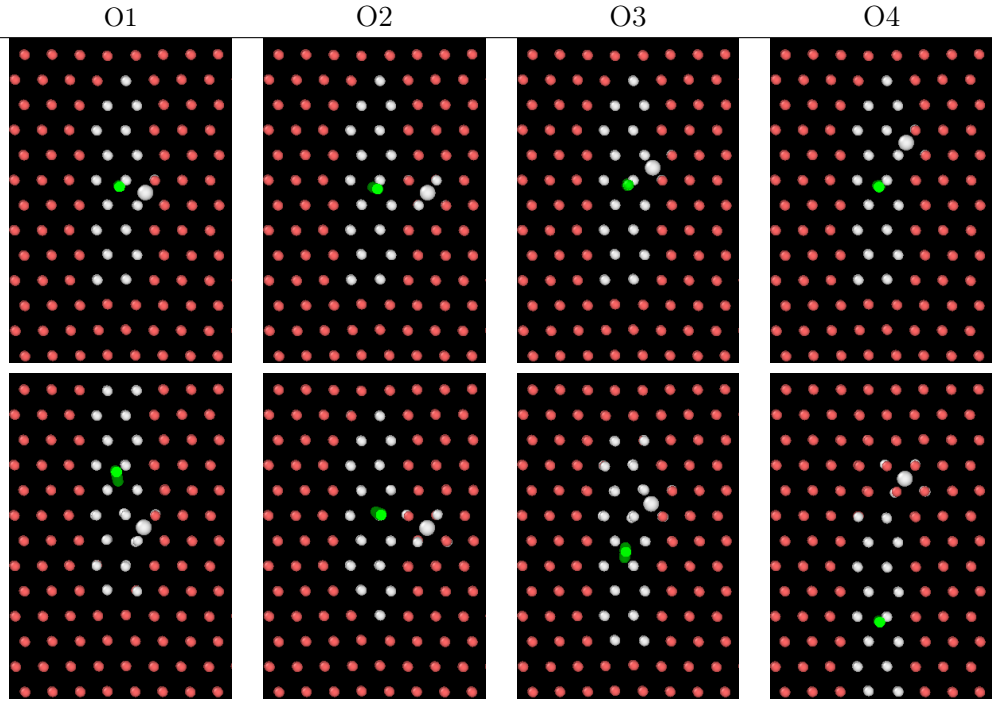


Table 4: Change in IP1 core structure and dislocation position upon addition of interstitial oxygen in different octahedral sites in a quadrupolar simulation. Row 1: Prior to relaxation. Row 2: After relaxation.

7.2 Notes

A strategy to find the binding energies of different interstitial sites.

1. Find cores of the dislocation using my in-house differential displacement map analysis.
2. Identify octahedral sites near the cores.
3. Translate octahedral sites from the perfect lattice to the lattice with a dislocation by the average displacement of the six surrounding lattice sites.
4. Put the solute into a given interstitial site such that upon application of the transformation of lattice from one dislocation core to another (upon rotation and reflection), the interstitial is in an equivalent position. (If one were to look at each dislocation in with the burgers vector pointing into the page, the site should be equivalent.)
5. Relax and find the binding energy by calculating the difference in energy from the relaxed dislocation to the unrelaxed.

7.3 Dissolution Energy Equation

The binding energy of oxygen to a dislocation can be given by the following equation:

$$E_{\text{O-disl.}}^{\text{sol}} = E_{\text{disl+}n\text{O}} - E_{\text{disl}} - \frac{n}{2}E_{\text{O}_2}$$

Here, the energy of molecular oxygen $E_{\text{O}_2}/2$ is -5.6eV/atom from Aksyonov 2016 [8].

7.4 Current status of simulation

An S-arrangement of dislocation dipoles was created in a 12x12 supercell of 576 atoms oriented such that the $1/3[11\bar{2}0]$ direction was parallel to the z axis. The dislocation cores were in the initial position 5 (IP5) and relaxed.

The cell was augmented by two extra periodic images in the z-direction, creating a 12x12x3 cell of 1728 atoms.

Oxygen was put into octahedral sites in increasing distance from each of the cores. The distance was up to four octahedral sites from the core along the prismatic plane and four prismatic planes along. This gives 16 sites from which one can extract the dependence of the dislocation binding energy with distance from the dislocation core.

These will provide references for the embedding calculations. It is hoped that embedding will give more accurate answers due to:

1. There only being one dislocation in an embedding cell:

- Dislocation strain fields are long-ranged, therefore one can expect errors due to the additional dislocation-dislocation interaction upon relaxation.

Unfortunately, it was seen with the addition of oxygen to both cores that the dipole configuration became unstable. Furthermore, the effective shear stress applied when an oxygen was near the dislocation core was enough to cause the dislocation to move on the prismatic plane.

8 Peierls Barriers

One can calculate the Peierls barrier to dislocation motion on particular planes by preparing two relaxed simulation cells, with the dislocation cores translated with respect to each other on the plane of interest.

Evidence from Clouet [4] suggests that such a dislocation core in this initial position (IP1) can undergo a locking and unlocking mechanism. A prismatically spread $\langle 11\bar{2}0 \rangle$ screw core can glide along the wide prismatic plane with a low shear stress, due to the small Peierls barrier on this plane. This glissile core is metastable, allowing for transformation to the ground state configuration of the dislocation (as found by DFT) which is a sessile, pyramidal spread core on the first-order pyramidal plane. This is the "locking" mechanism (whereas unlocking is the opposite: a sessile pyramidal to glissile prismatic core transformation). This core can then glide on the pyramidal plane by transformation into a glissile pyramidal spread core, which has a much higher Peierls barrier (and excess energy) than the prismatic glissile core, resulting in an increase in lattice friction dislocation on the pyramidal plane compared to the prismatic plane.

To calculate these Peierls barriers, first one considered the prismatic plane. The relaxed IP1 core is situated in a wide prismatic plane, which has a lower shear stress for glide activation than the narrow prismatic plane. The dislocation(s) of one cell were translated by $\frac{c}{2}$ in the y direction with respect to the other cell and relaxed.

For the basal plane, one translated the dislocation(s) by $\frac{\sqrt{3}a}{2}$ in the x direction.

For the pyramidal plane, one translated the dislocation by $[\frac{\sqrt{3}a}{2}, c]$.

9 BOP

9.1 4 recursion levels

$k_b T = 0.1$

» Lattice parameters:

> hcp

```

a      2.901660 Å
c      4.747485 Å
etot   -18.342162 eV

```

> omega

```

a      7.917318 Å
c      2.749892 Å
etot   -17.458700 eV

```

Omega is still not as stable as hcp as expected from model.

» Elastic Constants

Quantity	calc. (10^{11} Pa)	exp. (10^{11} GPa)
C11	1.781	1.761
C12	0.738	0.868
C13	0.611	0.682
C33	1.969	1.905
C44	0.285	0.508
C66	0.522	0.450
K	1.050	1.101
R	0.669	0.618
H	0.558	0.489

10 Bibliography

References

- [1] Nathalie Tarrat, Magali Benoit, and Joseph Morillo. Core structure of screw dislocations in hcp ti: an ab initio DFT study. *International Journal of Materials Research*, 100(3):329–332, mar 2009.
- [2] Emmanuel Clouet. Screw dislocation in zirconium: An ab initio study. *Physical Review B - Condensed Matter and Materials Physics*, 86(14):1–11, 2012.
- [3] Vasily Bulatov. *Computer Simulations of Dislocations (Oxford Series on Materials Modelling)*. Oxford University Press, dec 2006.
- [4] Emmanuel Clouet, Daniel Caillard, Nermine Chaari, Fabien Onimus, and David Rodney. Dislocation locking versus easy glide in titanium and zirconium. *Nature Materials*, 14(9):931–936, sep 2015.
- [5] M. Ghazisaeidi and D.R. Trinkle. Core structure of a screw dislocation in ti from density functional theory and classical potentials. *Acta Materialia*, 60(3):1287–1292, feb 2012.
- [6] P.M. Anderson, J.P. Hirth, and J. Lothe. *Theory of Dislocations*. Cambridge University Press, 2017.
- [7] Z M Chen, M Mrovec, and P Gumbsch. Atomistic aspects of \$\backslash case{1}{2}\backslash langle 1\backslash, 1\backslash, 1 \backslash rangle\$ screw dislocation behavior in-iron and the derivation of microscopic yield criterion. *Modelling and Simulation in Materials Science and Engineering*, 21(5):055023, June 2013.
- [8] D A Aksyonov, T Hickel, J Neugebauer, and A G Lipnitskii. The impact of carbon and oxygen in alpha-titanium:ab initio study of solution enthalpies and grain boundary segregation. *Journal of Physics: Condensed Matter*, 28(38):385001, July 2016.